HHS Public Access

Author manuscript

J Comp Neurol. Author manuscript; available in PMC 2018 May 01.

Published in final edited form as:

J Comp Neurol. 2017 May 01; 525(7): 1668–1684. doi:10.1002/cne.24158.

Descending Projections from the Basal Forebrain to the Orexin Neurons in Mice

Lindsay J Agostinelli[1], **Loris L Ferrari**[1], **Carrie E Mahoney**[1], **Takatoshi Mochizuki**[1], **Bradford B Lowell**[2], **Elda Arrigoni**[1,*], and **Thomas E Scammell**[1,*]

[1]Department of Neurology, Beth Israel Deaconess Medical Center and Harvard Medical School, Boston, MA 02215 USA

[2]Department of Medicine, Beth Israel Deaconess Medical Center and Harvard Medical School, Boston, MA 02215 USA

Abstract

The orexin (hypocretin) neurons play an essential role in promoting arousal, and loss of the orexin neurons results in narcolepsy, a condition characterized by chronic sleepiness and cataplexy. The orexin neurons excite wake-promoting neurons in the basal forebrain (BF), and a reciprocal projection from the BF back to the orexin neurons may help promote arousal and motivation. The BF contains at least three different cell types (cholinergic, glutamatergic, and GABAergic neurons) across its different regions (medial septum, diagonal band, magnocellular preoptic area, and substantia innominata). Given the neurochemical and anatomical heterogeneity of the BF, we mapped the pattern of BF projections to the orexin neurons across multiple BF regions and neuronal types. We performed conditional anterograde tracing using mice that express Cre recombinase only in neurons producing acetylcholine, glutamate, or GABA. We found that the orexin neurons are heavily apposed by axon terminals of glutamatergic and GABAergic neurons of the substantia innominata and magnocellular preoptic area, but there was no innervation by the cholinergic neurons. Channelrhodopsin-Assisted Circuit Mapping (CRACM) demonstrated that glutamatergic SI neurons frequently form functional synapses with the orexin neurons, but surprisingly, functional synapses from SI GABAergic neurons were rare. Considering their strong reciprocal connections, BF and orexin neurons likely work in concert to promote arousal, motivation, and other behaviors.

Graphical Abstract

Corresponding Author: Thomas E. Scammell, Beth Israel Deaconess Medical Center, Center for Life Science, Room 705, 330 Brookline Ave., Boston, MA 02215, Phone (617)-735-3260, Fax (617)-735-3252, tscammel@bidmc.harvard.edu.

*Co-senior authors

Conflicts of Interest: None of the authors have any conflicts.

Role of Authors:

All authors had full access to all the data in the study and take responsibility for the integrity of the data and the accuracy of the data analysis. Study concept and design: LJA, TS. Performed experiments: LJA and LF. Analysis and interpretation of data: LJA, BBL, LF, EA, TS. Drafting of the manuscript: LJA, TS, EA with comments from all authors. Critical revision of the manuscript for important intellectual content: LJA, TS, EA. Statistical analysis: LJA and LF. Obtained funding: TS, LJA. Administrative, technical, and material support: LJA, CEM, TM. Study supervision: TS, EA

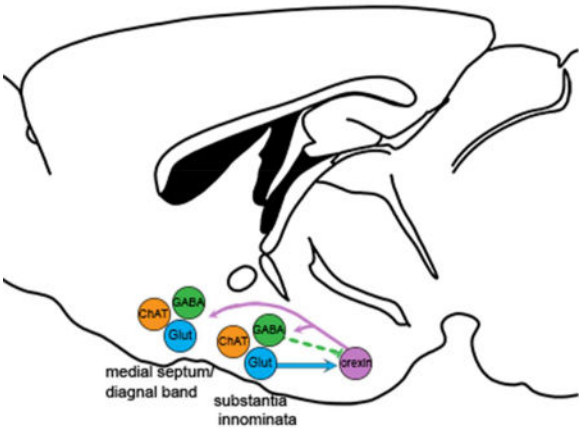

The basal forebrain and orexin neurons are both implicated in arousal and wakefulness. Glutamatergic projections from the substantia innominata (SI) strongly excite the orexin neurons, but GABA projections from the SI are generally silent. The medial septum (MS) and horizontal nucleus of the diagonal band (HDB) sparsely innervate the orexin neurons.

Keywords

substantia innominata; CRACM; anterograde; magnocellular preoptic; hypocretin; mice; lateral hypothalamus; RRID AB_653610; RRID AB_262156; RRID AB_10013483; RRID AB_11180610

INTRODUCTION

The basal forebrain (BF) is necessary for arousal, attention, and many other aspects of cognition (Fuller et al., 2011; Everitt and Robbins, 1997; Sarter et al., 2005; Ljubojevic et al., 2014; Voytko et al., 1994), and much research has focused on cholinergic BF projections to the cortex (Saper, 1984; Jones, 2004; Han et al., 2014; Goard and Dan, 2009; Pinto et al., 2013; Shi et al., 2015; Irmak and de Lecea, 2014). However, the BF also contains glutamatergic and GABAergic neuronal populations (Gritti et al., 2006; Zaborszky and Duque, 2003, Hur and Zaborszky, 2005; Xu et al., 2015) that extend throughout the length of the BF from the medial septum (MS), horizontal and vertical limbs of the diagonal bands (HDB and VDB), and back to the magnocellular preoptic nucleus (MCPO) and substantia innominata (SI).

In part, BF neurons likely drive arousal via ascending projections to the cortex (Rye et al., 1984; Gritti et al., 1997; Jones, 2004; Adamantidis et al., 2010; Han et al., 2014; Shi et al., 2015), but the MCPO and SI also strongly innervate the wake-promoting orexin (hypocretin) neurons in the lateral hypothalamus (LH) (Yoshida et al., 2006; Henny and Jones, 2006a) and other subcortical targets (Swanson et al., 1984; Semba, 2000). Orexin neurons are essential for maintaining wakefulness and regulating REM sleep, and extensive loss of the orexin neurons results in narcolepsy (Thannickal et al., 2000; Peyron et al., 2000; Chemelli et al., 1999) characterized by excessive daytime sleepiness and cataplexy. Many researchers have proposed that the orexin neurons promote arousal by exciting wake-active neurons in

the BF (Arrigoni et al., 2010; Fadel and Frederick-Duus, 2008; Jones, 2008; Saper et al., 2010), and we hypothesize that reciprocal projections from the BF back to the orexin neurons may further promote arousal and other shared functions.

Previous studies have examined these descending projections using conventional tracers, but these methods may have limited sensitivity as they require double immunolabeling of nerve terminals (Gautron et al., 2010). More importantly, prior research has not mapped whether these descending projections to the orexin neurons vary across BF nuclei or whether these pathways actually influence the activity of the orexin neurons. To map these descending projections to the orexin neurons, we used conditional anterograde tracing of BF neurons producing acetylcholine, GABA, or glutamate. We then tested the functions of these projections in vitro using Channelrhodopsin-Assisted Circuit Mapping (CRACM).

METHODS

Animals

We used female Cre-expressing mice weighing 20–30g, n=15–20 of each line. These recombinant mice have very similar designs, with an IRES-Cre cassette inserted just after the stop codon of the genes coding for choline acetyltransferase (Chat), vesicular glutamate transporter 2 (vGluT2), or vesicular GABA transporter (vGAT). The vGAT- and vGluT2-Cre mice have been previously validated and show excellent alignment of vGAT and vGluT2 mRNA with recombinase activity in a reporter line (Vong et al., 2011). Glutamate can be packaged into synaptic vesicles by vGluT1, vGluT2, or vGluT3, and in the BF, vGluT2 is the major vesicular glutamate transporter (Henny and Jones, 2006b; Harkany et al., 2003; Nickerson Poulin et al., 2006; www.alleninstitute.org). vGAT transports GABA into synaptic vesicles, and vGAT-Cre mice show recombination only in GABAergic neurons. The Chat-Cre mice have been validated in prior papers (Higley et al., 2011; Rossi et al., 2011).

We housed these mice on a 12:12 light:dark cycle with lights on at 0700 at 22 degrees C ambient temperature with *ad libitum* access to food and water. All protocols and care of the mice followed National Institute of Health guidelines and were approved by the Beth Israel Deaconess Medical Center Institutional Animal Care and Use Committee.

Conditional Anterograde Tracing

We used conditional anterograde tracing to map projections from the three major populations of BF neurons to the orexin neurons. We injected the BF of Cre-expressing mice with an adeno-associated viral vector (AAV8-EF1α-DIO-hChR2(H134R)-mCherry, 6×10^{12} pfu/ml, UNC Vector Core) coding for Cre-dependent channelrhodopsin (ChR2) tagged with the red fluorescent protein mCherry (AAV-ChR2-mCherry). In this AAV, the ChR2-mCherry sequence is inverted and surrounded by pairs of loxP and lox2272 sites, thus preventing non-specific expression of ChR2-mCherry. By injecting this AAV into mice that express Cre recombinase selectively in GABA (vGAT-Cre), glutamate (vGluT2-Cre), or acetylcholine (ChAT-Cre) neurons, ChR2-mCherry expression was limited just to neurochemically specific populations of BF neurons.

We anesthetized mice with ketamine/xylazine (100/10 mg/kg. i.p.) and unilaterally microinjected 3–6 nl of AAV-ChR2-mCherry into the BF. Injections were targeted at the major nuclei of the BF: medial septum (MS; AP +0.74, RL 0.09, DV −3.7 from the top of the skull); rostral part of the horizontal band of the diagonal band of Broca (HDB; AP +1.0, RL 0.45, DV −5.1); caudal part of the horizontal band of the diagonal band of Broca (HDB; AP +0.40, RL 1.1, DV −5.3); magnocellular preoptic nucleus (MCPO; +0.4, RL 1.25, DV −5.25); and substantia innominata (SI; AP −0.12, RL 1.80, DV −4.8). Researchers debate the definition of the SI (Canteras et al., 1995; Alheid, 2003; Heimer et al., 1997), and for simplicity, we use the term SI to describe the loosely packed, subcommissural group of neurons within the boundary of magnocellular cholinergic neurons dorsal to the more densely packed MCPO and HDB. Rostro-caudally, our SI injections ranged from the decussation of the anterior commissure back to the level of the caudal edge of the supraoptic nucleus.

Four weeks later, around 10:00am (3 hours after lights on), we deeply anesthetized mice with ketamine/xylazine (150/15 mg/kg ip) and transcardially perfused them with 50 ml phosphate-buffered saline (PBS; pH 7.4) followed by 50 ml of buffered 10% formalin (pH 7.0; Fisher Scientific, Fair Lawn, NJ). We removed and postfixed the brains for 12 hours in 10% formalin and then cryoprotected them in PBS containing 20% sucrose. We later coronally sectioned the brains at 30μm into a 1:4 series on a freezing microtome.

Immunohistochemistry

We defined the BF by the boundaries of the cholinergic population as others have done previously (Hedreen et al., 1984; Schwaber et al., 1987; Semba, 2000). To establish that AAV-ChR2-mCherry injections were within the borders of the BF, we double immunolabeled one series of sections from each mouse black for DsRed (which labels mCherry) and brown for ChAT with 3, 3'-diaminobenzidine (DAB) (Figure 1). Methodological details such as PBS washes were followed as described in Yoshida et al., 2006. In brief, we placed BF sections in 0.3% hydrogen peroxide prepared in PBT (phosphate-buffered saline (PBS), pH 7.4 with 0.25% Triton X-100) for 30 minutes to inactivate endogenous peroxidases and then incubated them overnight in rabbit anti-DsRed (Clontech, Cat# 632496, RRID AB_10013483, rabbit, polyclonal) and goat anti-ChAT (Millipore, Cat# AB144P, RRID AB_262156, goat, polyclonal) prepared in PBT with normal horse serum (Table 1). The next day, we incubated sections for 1 hour in biotinylated donkey anti-rabbit IgG secondary antiserum (1:500; Jackson ImmunoResearch; catalog #711-065-152) followed by one hour in avidin-biotin complex (ABC) (Vectastain ABC Elite Kit; Vector Laboratories, Burlingame, CA). We labeled mCherry black with DAB in tris-buffered saline (TBS) with 0.024% hydrogen peroxide solution and 0.2% ammonium nickel (II) sulfate. To visualize ChAT, we placed sections for 1 hour in biotinylated donkey anti-goat IgG secondary antiserum (1:500; Jackson ImmunoResearch; catalog #705-065-147) followed by one hour in ABC, and stained brown with DAB in TBS with 0.024% hydrogen peroxide.

To visualize the BF innervation of orexin neurons, we double immunolabeled one series of sections black for mCherry and brown for orexin-A with DAB. We placed lateral

hypothalamic sections in 0.3% hydrogen peroxide for 30 minutes and then incubated them overnight in rabbit anti-DsRed and goat anti-orexin-A (Santa Cruz Biotechnology, Cat# sc-8070, RRID AB_653610, goat, polyclonal). We stained the DsRed black with nickel-DAB, followed by staining orexin-A brown with DAB, as described above.

To analyze BF innervation of the orexin field with confocal microscopy, we fluorescently double-labeled sections for DsRed and orexin. We incubated hypothalamic sections overnight in rabbit anti-DsRed (1:2,000) and goat anti-orexin-A. Then we placed sections in donkey anti-rabbit IgG conjugated to Alexa Fluor 555 (1:1000; Invitrogen; catalog #A31572) and donkey anti-goat IgG conjugated to Alexa Fluor 488 (1:1000; Invitrogen; catalog #A11055) for one hour to stain mCherry-containing terminals red and orexin neurons green.

After DAB or fluorescent immunolabeling, we mounted and air dried sections on Superfrost Plus slides. For sections with fluorescence immunolabeling, we coverslipped with fade-retardant aqueous mounting medium containing DAPI (Vectashield; Vector Labs). For DAB-labeled tissue, we dehydrated sections in graded ethanols for three minutes each and cleared them in xylenes for over an hour before coverslipping with a toluene-based mounting media (Cytoseal; Thermo Scientific). The final thickness of these dehydrated sections was approximately 12–15 μm.

The GFP and DsRed antisera produced no labeling in wild type mice lacking these peptides, and the orexin antisera produced no staining in orexin knockout mice.

Validation of Neurochemical Specificity

To confirm that mCherry was expressed only in the correct types of neurons, we immunolabeled BF sections for mCherry and markers of cholinergic, glutamatergic, and GABAergic neurons.

We incubated BF sections from ChAT-Cre mice overnight in rabbit anti-DsRed (1:2,000) and goat anti-ChAT (1:1,000). The next day, we incubated sections for 1 hour in donkey anti-rabbit IgG conjugated to Alexa Fluor 555 and donkey anti-goat IgG conjugated to Alexa Fluor 488 to label mCherry neurons red and ChAT neurons green (Figure 2). We imaged whole sections using an Olympus VS120 slide scanner at a final magnification of 200×, and used a z-stack at 1 μm intervals to image through the section. We viewed stacks of images using OlyVIA software and counted double-labeled cells. In the Chat-Cre tissue, 100% of neurons that expressed mCherry were also immunolabeled for ChAT.

In the vGluT2-Cre and vGAT-Cre mice, we performed in situ hybridization histochemistry (ISHH) for vGluT2 and vGAT mRNA, respectively, followed by immunolabeling for marker proteins. We rinsed the brain sections in DEPC-PBS and then incubated the tissue in hybridization buffer (50% formamide, Fisher; 5× SSC, Promega; 0.5 mg/mL t-RNA, Roche; 5% dextran, Sigma; 1× Denhardt's solution, Sigma; 0.1% Tween-20, Sigma; DEPC-water) for one hour at 54°C. The DIG-RNA vGAT (542bp, refer to NM_009508.2, bp 874 to 1416) and vGluT2 probes (458bp, refer to NM_080853.3; bp829 to 1287) were transcribed from a pGEM-TEasy plasmid. We linearized the plasmid with Sac1 (New England Labs) and

transcribed riboprobes with T7 polymerase (Roche) in the presence of digoxigenin-conjugated UTP (Roche, DIG RNA labeling mix #11277073910). Digoxigenin-labeled anti-sense riboprobe (300 ng/μL probe) was added to each well and incubated at 54°C overnight.

We washed the tissue in 2× SSC in 50% formamide for 45 min at 54 C, followed by two 30 min washes in 2× SSC. Non-hybridized RNA probes were eliminated with an RNaseA step: sections were washed twice for 5min at room temperature in RNase buffer (0.5 M NaCl and 10 mM Tris-HCl) before and after a 30 min incubation at 37 C in RNase A (50 μg/mL). We washed the sections in 2× SSC (5 min at room temperature), then 2× SSC-50% formamide (5 min at 54 C), followed by 1× SSC-50% formamide in DEPC-H2O (5 min ×2 at room temperature), and then TBS (5 min ×3 at room temperature). We incubated the sections in Roche's Boehringer Blocking Reagent (diluted to 5% w/v in TBS with 0.1% Tween, dissolved for 5 min) at 54 C for 30 min. We next added anti-digoxigenin-POD Fab fragments (Roche #11-207-733-910; lot# 14299300) to this blocking solution at a 1:200 dilution for overnight incubation at room temperature. We washed the sections in TBS 3 times for 10 minutes each in preparation for the fluorescence tyramide signal amplification (TSA) step. We incubated the tissue for 30 min at room temperature in a solution of biotinylated tyramide solution (Perkin-Elmer #FP1019, lot #1673734) diluted 1:50 in solution #FP1050 (lot #1734999). We washed the tissue in TBS (5 min), PBS (rinse), PBS (10 min), and then PBT (2 hours), and incubated the tissue in streptavidin-Alexa Fluor 488 (1:1,000; Invitrogen; catalog #S11223) for 2 hours at room temperature to label the mRNA green. For the electrophysiology experiments (described below) we used AAV-ChR2-YFP, so we labeled mRNA red with streptavidin-Alexa Fluor 555 (1:1,000; Invitrogen; catalog #S32355). We then washed sections three times in PBS for 5 min each.

After the ISHH, we incubated the sections overnight in rabbit anti-DsRed to label the ChR2-mCherry and then placed sections in donkey anti-rabbit IgG conjugated to Alexa Fluor 555 as above to label soma red. We found that 91% and 98% of the mCherry-labeled cells were also labeled for vGluT2 and vGAT, respectively. For electrophysiology experiments, we used AAV-ChR2-YFP, so after ISHH, we incubated sections overnight with chicken anti-GFP (Life Technologies, A10262, RRID AB_11180610, polyclonal) (which binds YFP) followed by donkey anti-chicken IgG conjugated to Alexa Fluor 488 (1:500; Jackson ImmunoResearch; catalog #703-545-155) for one hour to stain YFP-containing soma green. We then imaged tissue using a confocal microscope and counted cells. We found that 93% and 99% of the YFP-labeled cells were also labeled for vGluT2 and vGAT, respectively. For Figure 2, we collapsed the stacks into one image using the Z Project function in ImageJ.

To establish that the BF vGAT and vGluT2 neurons are distinct from the cholinergic neurons, we used double fluorescent immunolabeling with rabbit anti-DsRed and goat anti-ChAT in BF sections from vGAT and vGluT2-Cre mice injected with AAV-ChR2-mCherry, followed by one hour in donkey anti-rabbit IgG conjugated to Alexa Fluor 555 and donkey anti-goat IgG conjugated to Alexa Fluor 488 to label mCherry neurons red and ChAT neurons green.

Analysis of Anterograde Tracing

We targeted our injections at the MS, HDB, MCPO, or SI and then selected cases that were limited to each part of the BF (n=3 for each region and for each Cre line). Criteria for inclusion were that the injection was confined to the boundaries of the cholinergic BF neurons. We excluded 7/47 cases as misses and used them as anatomical controls to contrast with BF injections. These controls included injections in the globus pallidus and preoptic area.

We plotted injection sites onto template drawings representing three levels of the BF (Figure 3). Specifically, we scanned BF sections using brightfield on a slide scanner (Olympus VS120; UPlanSApo 10× objective, 0.40 numerical aperture (NA)) and traced the center of the injection site onto a template using Photoshop (Adobe). The center of the injection site was defined as the section in the middle of the rostrocaudal extent of the injection, and then we traced around the entire border of the transfected cells.

To quantify the innervation of orexin neurons, we counted the number of orexin neurons apposed by mCherry-labeled synaptic boutons. First, we selected sections from the rostral, central, and caudal parts of the orexin field spaced 240 μm apart (Figure 4A). To determine if a cell was apposed by a nerve terminal from the BF, we examined each orexin neuron containing a nucleus using brightfield microscopy (Zeiss Axioplan 2; 100× oil objective (Plan-Neofluar 1.3 NA) with a Zeiss achromatic-aplanatic universal condenser 0.9), adjusting the focus to maximize visibility of appositions. An orexin neuron was considered innervated if there was at least one mCherry-labeled bouton immediately adjacent to the soma or proximal dendrites (Figure 4B). On a photomicrograph of the section, we marked each orexin neuron with a blue dot if it was innervated or a red dot if it was not (Figure 5). To examine regional changes across the orexin field, we counted appositions in the three rostral-caudal levels and also in the lateral, perifornical, and medial parts of the orexin field.

Confocal Microscopy and Analysis

We used confocal microscopy to confirm that BF neurons form close appositions on orexin neurons. First, we fluorescently labeled LH sections green for orexin and red for the mCherry-filled BF terminals. We then photographed double-labeled sections in 1μm optical sections using a Zeiss LSM 510 META confocal microscope with a Zeiss Plan-ApoChromat 63× oil objective (1.4 NA). We scrolled through the 20 z-stack images using ImageJ (NIH, Bethesda, MD) and counted orexin neurons that received at least one BF apposition immediately adjacent to the soma and proximal dendrites. We used Photoshop to adjust brightness and contrast when needed, and in some images, we pseudo-colored red as magenta.

Synaptophysin Labeling

To establish further whether the anatomical appositions form synapses, we labeled presynaptic terminals with mCherry fused to synaptophysin, a presynaptic vesicle glycoprotein (Rizzoli, 2014). Using the same three lines of mice, we injected the SI with an AAV coding for Cre-dependent synaptophysin fused to mCherry (AAV8-hEF1α-DIO-synaptophysin-mCherry-WPRE) (Garfield et al., 2014). After four weeks, we perfused the

mice and immunostained mCherry black with DAB-Ni and orexin neurons brown with DAB, using the protocol described above. The synaptophysin-mCherry produced black punctate labeling of synaptic boutons with minimal labeling of axons, and we counted synaptophysin-immunolabeled boutons apposing orexin neurons as described above using the 100× oil objective.

Channelrhodopsin-Assisted Circuit Mapping (CRACM)

To confirm that projections from the BF form functional synapses onto orexin neurons, we used *in vitro* CRACM with dual AAV injections. We unilaterally microinjected the SI of 7–9 week old vGAT-Cre ($n = 7$ mice) and vGluT2-Cre ($n = 7$ mice, but 2 were excluded for missed injection sites) female mice with 3–6 nl of an AAV coding for ChR2 fused to enhanced yellow fluorescent protein (EYFP; AAV10-EF1α-DIO-hChR2(H134R)-EYFP; 1×10^{12} pfu/ml; a kind gift of the Fuller Lab)(Chen et al., 2015). This conditional YFP labeled BF soma and terminals as strongly as the mCherry labeling used in other experiments. To identify the orexin neurons in recording slices, we also injected the orexin field with an AAV in which a 1.3 kb fragment of the human prepro-orexin promoter drives expression of tdTomato (AAV8-horexin-tdTomato; 1.7×10^{13} pfu/ml); the AAV construct was a kind gift of Takeshi Sakurai, Kanazawa Univ. (Saito et al., 2013). We unilaterally targeted 15 nl AAV injections at the medial and lateral parts of the orexin field (AP: 1.53mm, DV: −5.1mm, ML: 0.8 and 1.2). We recorded 25 orexin neurons from across the medial-lateral extent of the orexin field in 5 vGluT2-Cre mice. We recorded 46 neurons (39 orexin neurons + 7 non-orexin neurons) in 7 vGAT-Cre mice. We recorded an average of 5–7 neurons per mouse.

To determine if AAV-horexin-tdTomato labels only orexin neurons, we fluorescently immunolabeled LH sections for DsRed and orexin, and found that 82% of the tdTomato-labeled neurons were also double-labeled for orexin. The tdTomato-labeled neurons lacking orexin were small (<10 μm) and ventral and lateral to the orexin field. Therefore, our recordings targeted only large (>20 μm) tdTomato-labeled neurons in the orexin field, and all had the typical physiological characteristics previously described for orexin neurons (Schone et al., 2011).

Eight weeks after AAV injections, we prepared LH slices for electrophysiological recordings. We deeply anesthetized mice with isoflurane via inhalation around 10:00am (3 hours after lights on), and transcardially perfused them with ice-cold cutting ACSF (*N*-methyl-D-glucamine, NMDG-based solution) containing (in mM): 100 NMDG, 2.5 KCl, 1.24 NaH_2PO_4, 30 $NaHCO_3$, 25 glucose, 20 HEPES, 2 thiourea, 5 Na-L-ascorbate, 3 Na-pyruvate, 0.5 $CaCl_2$, 10 $MgSO_4$ (pH 7.3 with HCl when carbogenated with 95% O_2 and 5% CO_2). We quickly removed the mouse brains and sectioned them in coronal slices (250 μm thick) in ice-cold cutting ACSF using a vibrating microtome (VT1000S, Leica, Bannockburn, IL, USA). We transferred the slices containing the orexin field to normal ACSF containing (in mM): 120 NaCl, 2.5 KCl, 1.3 $MgCl_2$, 10 glucose, 26 $NaHCO_3$, 1.24 NaH_2PO_4, 4 $CaCl_2$, 2 thiourea, 1 Na-L-ascorbate, 3 Na-pyruvate (pH 7.4 when carbogenated with 95% O_2 and 5% CO_2, 310–320 mOsm).

We recorded from large neurons across the orexin field that expressed tdTomato using a combination of fluorescence and infrared differential interference contrast (IR-DIC) video microscopy. As controls, we also recorded from non-orexin neurons lacking tdTomato that lay within the orexin field. For these recordings, we used a fixed stage upright microscope (BX51WI, Olympus America Inc.) equipped with a 40× Olympus Nomarski water immersion objective (0.8 NAW) and IR-sensitive CCD camera (ORCA-ER, Hamamatsu, Bridgewater, NJ, USA), and we used AxioVision software (Carl Zeiss MicroImaging) to acquire real time images. We recorded in whole-cell configuration using a Multiclamp 700B amplifier (Molecular Devices, Foster City, CA, USA), a Digidata 1322A interface, and Clampex 9.0 software (Molecular Devices). We photostimulated BF axons and synaptic terminals expressing ChR2 using full-field 5ms flashes of light (~ 10 mW/mm^2, 1mm beam width) from a 5 W LUXEON blue light-emitting diode (470 nm wavelength; #M470L2-C4; Thorlabs, Newton, NJ, USA) coupled to the epifluorescence pathway of the microscope. We used a three light pulse protocol at 3 Hz, and we repeated this protocol every 5 sec (0.5 Hz) for 30 trials. For most of our recordings, we used a K-gluconate based pipette solution containing (in mM): 120 K-gluconate, 10 KCl, 3 $MgCl_2$, 10 HEPES, 2.5 K-ATP, 0.5 Na-GTP (pH 7.2 adjusted with KOH; 280 mOsm), that allowed us to verify the firing properties of the recorded cells. We recorded photo-evoked excitatory postsynaptic currents (EPSCs) in slices from vGluT2-Cre mice at Vh = −60 mV in ACSF using a K-gluconate-based pipette solution. We initially recorded photo-evoked inhibitory postsynaptic currents (IPSCs) with a K-gluconate based pipette solution in slices from one mouse (Vh = −40 mV in ACSF; Cl^- reversal potential = −64 mV), then with a Cs-methane-sulfonate-based pipette solution in slices from two mice (Vh = 0 mV in ACSF; Cl^- reversal potential = −64 mV), and then with a KCl-based pipette solution from 4 mice (Vh = −60 mV in ACSF + kynurenic acid 1 mM; Cl^- reversal potential = 1.77 mV). Composition of the Cs-methane-sulfonate-based pipette solution was (in mM): 125 Cs-methane-sulfonate, 11 KCl, 10 HEPES, 0.1 $CaCl_2$, 1 EGTA, 5 Mg-ATP and 0.3 Na-GTP (pH adjusted to 7.2 with CsOH 280 mOsm). Composition of the KCl-based pipette solution was (in mM): 140 KCl, 1 MgCl2, 10 HEPES, 1 EGTA, 0.3 CaCl2, 5 Mg-ATP, 0.3 Na-GTP (pH adjusted to 7.2 with KOH, 280 mOsm). To record photo-evoked synaptic events in the presence of tetrodotoxin (TTX; 1 μM), we bath applied the potassium blocker, 4-AP (1 mM) (Hull et al., 2009). We identified orexin neurons by expression of td-Tomato and confirmed this based on their firing properties (Schone et al., 2011).

We analyzed the electrophysiological data using Clampfit 9.0 (Molecular Devices) and IGOR Pro 6 (WaveMetrics, Lake Oswego, OR, USA). We analyzed the synaptic events off-line using Mini Analysis 6 (Synaptosoft, Leonia, NJ, USA). We calculated the latency of the photo-evoked EPSCs and IPSCs as the time difference between the start of the light pulse and the 5% rise point of the first EPSC (Hull et al., 2009).

Statistics

We report data as mean ± SEM. We used the Kruskal–Wallis rank sum test to compare cell counts between different levels of the orexin field, followed by a Dunn's multiple comparison test to identify significant pairwise differences (StatView; SAS Institute, Cary, NC).

RESULTS

1. Conditional anterograde tracing

We injected AAV-ChR2-mCherry into the BF of ChAT-Cre, vGluT2-Cre, and vGAT-Cre mice. The injection sites were small, with typical diameters of 720– 960 μm (Figure 1). We double-labeled sections for mCherry and ChAT, and selected 3 cases limited to the MS, HDB, MCPO, or SI for each of the three lines of mice (Figures 2 and 3). In ChAT-Cre mice, all mCherry-containing neurons also labeled for ChAT. In vGluT2-Cre and vGAT-Cre mice, mCherry never co-localized with ChAT, demonstrating that the vGAT and vGluT2 neurons are distinct from the cholinergic neurons as indicated in prior studies (Gritti et al., 2006; Xu et al., 2015).

This method produced robust and selective anterograde labeling in GABAergic, glutamatergic, and cholinergic BF neurons, with the heaviest innervation of the orexin field arising from the lateral and caudal parts of the BF (SI and MCPO). We estimated the percentage of orexin neurons innervated by each BF cell type by counting the number of orexin neurons with at least one closely apposing bouton from each of the different BF areas (Figure 4, Table 2). While the identification of a single apposition on orexin neurons provided a minimal criterion for counting a neuron targeted by each BF region, most orexin neurons were apposed by multiple GABAergic and glutamatergic boutons. The GABAergic and glutamatergic neurons also formed ascending projections to the cortex, hippocampus, and amygdala plus descending projections to many additional regions including the posterior hypothalamus, supramammillary nucleus, habenula, VTA, and parabrachial nucleus that we will describe in a separate report.

2. Innervation of the orexin neurons by the substantia innominata

Among the BF regions, the SI most densely innervated the orexin neurons. Injections in the caudal SI at the level of the posterior part of the anterior commissure (Figure 3A3, 3B3) formed mostly ipsilateral projections, with axons descending through the medial forebrain bundle. A large part of this projection terminated in the LH, though many axons continued on to more caudal regions. In the hypothalamus, fibers were densest in the lateral portion of the LH adjacent to the internal capsule, extended medially across the orexin neuron field, and heavily terminated in the lateral posterior hypothalamus (LHp); fibers were sparser in medial regions such as the paraventricular nucleus (PVH), ventromedial hypothalamus, and dorsomedial nucleus (DMH). Both GABAergic and glutamatergic SI neurons densely innervated the orexin field, but cholinergic fibers in the orexin field were completely absent.

Over the entire orexin field, the GABAergic and glutamatergic boutons originating from the SI formed close appositions on 89%± 3 and 80%± 1 of the orexin neurons, respectively (Figure 5 and Table 2). The conditional tracing method also worked well in the cholinergic BF neurons, producing heavy labeling of axons to the cortex, hippocampus, basolateral amygdala, and other regions. However, within the orexin field, cholinergic axons were absent, and we found no orexin neurons with cholinergic appositions from the BF.

The medial and lateral parts of the orexin field are hypothesized to mediate different functions (Estabrooke et al., 2001; Harris and Aston-Jones, 2006; Yoshida et al., 2006) so

we subdivided our mapping of glutamatergic and GABAergic appositions on orexin neurons into three medial to lateral divisions and three rostral-caudal levels. Boutons from GABAergic SI neurons formed close appositions on orexin neurons across the lateral, perifornical, and medial parts of the orexin field (95% ± 2%, 91% ± 3%, 84% ± 3%; p=0.11) (Figure 5). In contrast, glutamatergic innervation was strong in the lateral field and moderate medially (91% ± 1%, 79% ± 1%, 63% ± 2%; p=0.03); pairwise comparisons showed significant differences between the lateral and medial divisions ($p<0.05$). Across the rostral, mid, and caudal levels of the orexin field, there was little variation in the GABAergic innervation (91% ± 2%, 90% ± 3%, 87% ± 5%), and glutamatergic innervation (77% ± 2%, 79% ± 1%, and 85% ± 5%) of the orexin neurons.

Synaptophysin is a reliable marker of presynaptic protein complexes (Rizzoli, 2014), and the frequency of appositions on orexin neurons was similar in mice with AAV-synaptophysin-mCherry injected into the SI. Specifically, 79% and 77% of orexin neurons received mCherry-labeled boutons in vGluT2-Cre and vGAT-Cre mice, respectively, but there were no appositions in ChAT-Cre mice. The slightly lower numbers of appositions with this method may be due to lower transduction efficiency with this AAV or fewer false positive appositions than in the ChR2 sections in which irregularities in axons occasionally resemble axon boutons.

We analyzed all confocal images to determine if the BF boutons labeled with ChR2-mCherry form close appositions on the orexin neurons. We acquired 20 images per z-stack and examined each 1 um optical section for appositions. We acquired images in the lateral, perifornical, and medial aspects of the orexin field. We found that about 78% and 80% of the orexin neurons received glutamatergic and GABAergic appositions, respectively.

3. Innervation of the orexin neurons by other BF regions

Innervation of the orexin neurons varied greatly across BF regions. GABAergic and glutamatergic neurons of the MCPO innervated the orexin neurons almost as heavily as those of the SI, but innervation from the HDB and MS was light (Figure 6, Table 2). Unlike projections from the SI, none of these BF regions showed statistically significant topographical variations across the medial-lateral extent of the orexin field. No BF region showed variations in apposition density along the rostral-caudal extent of the orexin field. Across all BF regions, cholinergic neurons did not innervate the orexin neurons.

Each BF region projected to the orexin field via moderately distinct descending pathways, and GABAergic and glutamatergic BF neurons followed similar paths. Sparse, descending projections from the MS mostly ran adjacent to the optic tract with a few axons running through the medial forebrain bundle, innervating only 1–2% of the orexin neurons. The rostral and caudal HDB innervated mainly orexin neurons in the ventral part of the orexin field (GABAergic and glutamatergic boutons opposed about 5% and 9% of the orexin neurons, respectively), with fibers descending in a pattern similar to those of the MS. These HDB injections extended slightly into the rostral SI or MCPO which likely increased the apparent density of this projection. Fibers from the MCPO projected through the medial forebrain bundle to the orexin neurons, mainly innervating the mid- and ventral parts of the

orexin field. The SI innervated the entire orexin field, with especially heavy innervation of the dorsal part.

We placed control injection in the ventromedial globus pallidus (just dorsal to the SI), and we did not see projections to the orexin field. Control injections into the lateral and medial preoptic area revealed strong projections to the ventral orexin field, so in analyzing our BF series, we excluded cases with any extension of tracer medial to the BF.

4. ChR2-assisted circuit mapping (CRACM) of SI-to-orexin projections

We used CRACM to test for synaptic connectivity between glutamatergic and GABAergic neurons of the SI and the orexin neurons (Figure 7). We injected AAV-ChR2-EYFP virus in the SI region and AAV-horexin-tdTomato in the perifornical region of vGluT2-Cre mice and vGAT-Cre mice. YFP expression was limited to glutamatergic or GABAergic neurons of the SI, and tdTomato was strongly expressed in the orexin neurons.

Photostimulation of SI glutamatergic axons and terminals evoked release of glutamate and firing of orexin neurons. In voltage-clamp recordings, photostimulation of glutamatergic projections rapidly evoked excitatory postsynaptic currents (EPSCs) in 23/25 recorded orexin neurons (peak amplitude of the photo-evoked EPSCs: 36.35 ± 5.18 pA). This effect was blocked by DNQX (20 μM), indicating that these responses were mediated by postsynaptic AMPA receptors. The EPSCs had short latencies (4.92 ± 0.21 ms; $n = 23$) and were maintained in TTX (n = 6) suggesting direct monosynaptic connectivity between SI glutamatergic terminals and the orexin neurons. Additionally, we did not see IPSPs after photostimulation, indicating no release of GABA from the BF terminals in vGluT2-Cre mice.

In contrast, photostimulation of GABAergic projections rarely evoked postsynaptic responses in orexin neurons. Initially, we recorded from orexin neurons using a K-gluconate-based pipette solution ($n = 5$ neurons) or a Cs-methane-sulfonate-based pipette solution ($n = 8$). Orexin neurons demonstrated spontaneous inhibitory postsynaptic currents (IPSCs) that were blocked by bicuculline (10 μM), but these events were not synchronized to photostimulation. As a positive control, we recorded from non-orexin neurons within the orexin field and found short latency (5.44 ± 0.74 ms) evoked IPSCs in 4/7 neurons. We then recorded from an additional 26 orexin neurons using a KCl-based pipette solution to increase the detection of photo-evoked IPSCs. Under this condition, we found that photostimulation of GABAergic projections evoked IPSCs in 4/26 recorded orexin neurons (IPSC latency: 4.68 ± 1.18 ms and IPSC peak amplitude: 60.59± 42.9pA). Additionally, we did not see EPSCs after photostimulation under any conditions, indicating no release of glutamate from the BF terminals in vGAT-Cre mice. These results demonstrate that photostimulation of SI GABAergic terminals can evoke release of GABA onto the orexin neurons, but the number of functional synapses is low.

DISCUSSION

We examined whether BF neurons innervate the orexin neurons as both regions likely work in concert to promote arousal and other behaviors. Conditional anterograde tracing with

AAV-ChR2-mCherry demonstrates that glutamatergic and GABAergic neurons of the BF densely project to the orexin neurons of mice, but cholinergic BF neurons do not innervate the orexin neurons or other parts of the LH. These projections are topographic, with heavy innervation from the lateral parts of the BF, especially the caudal MCPO and SI, but sparse innervation from the medial parts of the BF. In addition, CRACM shows that glutamatergic neurons of the SI monosynaptically excite the orexin neurons, but despite the presence of numerous appositions, GABAergic BF neurons form few functional synapses on the orexin neurons. These findings suggest that feedback from BF glutamate neurons may regulate orexin neuron activity, but the GABAergic BF neurons appear to have little direct effect.

Pattern of SI BF projections to the orexin neurons

The descending glutamatergic and GABAergic projections from the SI and MCPO densely innervate the LH. We found that the SI glutamatergic input is heaviest in the lateral part of the orexin field, but the GABAergic projection from the SI is uniformly strong across the entire orexin field. Studies investigating functional divisions among orexin neurons suggest that more medial orexin neurons are involved with arousal, whereas lateral orexin neurons are involved in reward-seeking behaviors (Harris et al., 2005; Harris and Aston-Jones, 2006; Estabrooke et al., 2001; Fadel et al., 2002). In addition, non-cholinergic BF neurons fire in association with changes in sleep/wake states and also encode motivational salience (Hassani et al., 2009; Lin and Nicolelis, 2008; Raver and Lin, 2015). Perhaps the BF glutamatergic innervation of the orexin neurons that we describe mainly reinforces reward seeking or motivated behaviors.

To confirm that these ChR2-mCherry appositions were true synaptic specializations, we used another conditional tracer in which mCherry is fused to synaptophysin and found that 79% and 77% of the orexin neurons received appositions from SI glutamatergic and GABAergic neurons, respectively. For comparison, ChR2-mCherry labeled glutamatergic and GABAergic appositions on 80% and 89% of the orexin neurons. The slightly lower numbers of appositions with the synaptophysin method may be due to lower transduction efficiency with this AAV or fewer false positive appositions than in the ChR2 sections in which irregularities in axons occasionally resemble axon boutons.

Variations in projections from different BF nuclei

We find that the heaviest BF projections to the orexin neurons arise from the most lateral and caudal parts of the BF, but innervation from medial and rostral BF regions is sparse to nonexistent. In fact, the lateral-medial dimension may be most important as innervation is light from medial but relatively caudal regions such as the caudal HDB but moderately strong from the lateral but rostral part of the SI (data not shown). This pattern is in keeping with prior tracing studies in rats which showed moderate input to the orexin neurons from the SI but minimal to no input from the MS and HDB (Yoshida et al., 2006; Grove, 1988).

Our small injections into specific BF regions further demonstrate the anatomical heterogeneity among BF subnuclei, especially the differences between the MCPO and HDB. These adjacent structures are defined by loose clusters of magnocellular cholinergic neurons (Dinopoulos et al., 1986; Brashear et al., 1986), but their boundaries can be indistinct and

they are often considered together. We find that neurons in the HDB innervate very few orexin neurons whereas slightly more lateral neurons in the MCPO form strong projections. These distinctions highlight the general topology of the hypothalamus and BF proposed by Swanson and others which emphasizes anatomically and functionally distinct medial and lateral “columns” such that the lateral parts of the BF and the LH are anatomically and functionally linked (Swanson, 2000).

While only the lateral parts of the BF innervate the orexin neurons, the orexin neurons innervate the entire BF including the medial septum (Peyron et al., 1998), with preferential innervation of the BF from the medial orexin neurons (España et al., 2005). All BF regions express orexin receptors (Marcus et al., 2001), and orexins (orexin-A and orexin-B) excite cholinergic and non-cholinergic BF neurons in the medial septum, HDB, and MCPO (Eggermann et al., 2001; Wu et al., 2004; Arrigoni et al., 2010). In addition, microinjection of orexin-A into the MS or SI rapidly increases wake (España et al., 2001; Thakkar et al., 2001), even in the absence of cholinergic neurons (Blanco-Centurion et al., 2006). Thus, orexins excite cholinergic and non-cholinergic neurons across the BF, but feedback from the BF arises only from non-cholinergic neurons of the SI and MCPO. This asymmetry suggests that while the orexin neurons activate the entire BF, functions are segregated across the BF. Specifically, reciprocal connections between the lateral BF and orexin neurons may reflect shared roles in regulating arousal, motivation, and other functions.

Comparison and contrast with prior research

Henny and Jones (2006) mapped the projections from SI and MCPO to the orexin neurons in rats using injections of biotinylated dextran amines (BDA), and then double labeling boutons for neurochemical markers. They found that 41% of the orexin neurons within the lateral hypothalamus were contacted by BDA-positive appositions, and of these neurons, 31% and 67% had appositions positive for VGlut2 and VGAT, respectively. This would suggest that roughly 13% and 27% of the LH orexin neurons receive glutamatergic and GABAergic innervation from the BF, respectively, and even less if one considers the less heavily innervated orexin neurons in the perifornical region and dorsomedial nucleus. Furthermore, Henny and Jones reported post-synaptic scaffolding proteins on an even smaller percentage of orexin neurons, suggesting the connectivity is even lower. Using conditional tracing in mice, we found more numerous glutamatergic and GABAergic appositions (~80% and 90%, respectively) on the orexin neurons. This difference in intensity of innervation could be due to species differences, size of injections, and location with the BF, but we suspect that conditional tracing is more sensitive as conditional tracing produces large amounts of marker protein, and the method does not require double or triple labeling of nerve terminals. Future experiments should be able to establish which method is more sensitive by direct comparison of conditional and conventional tracers.

Though projections from glutamatergic and GABAergic BF neurons are very strong, we found that BF cholinergic neurons do not innervate the orexin neurons. One study using transgenic mice reported that cholinergic BF neurons innervated the orexin neurons (Sakurai et al., 2005), but this may have been a methodological artifact as other studies using conventional anterograde and retrograde tracers found very little to no innervation by BF

cholinergic neurons (Gritti et al., 1994; Henny and Jones, 2006a). The orexin neurons are excited by the cholinergic agonist carbachol (Bayer et al., 2005; Yamanaka et al., 2003; Ohno et al., 2008), but these cholinergic signals likely arise from other regions such as the pedunculopontine tegmental nucleus or the laterodorsal tegmental nucleus (Hallanger and Wainer, 1988; Satoh and Fibiger, 1986; Semba et al., 1988).

Possible functions of the glutamatergic BF projection

Our study provides strong evidence that glutamatergic MCPO and SI neurons can excite the orexin neurons. Henny and colleagues found that some orexin neurons contain the postsynaptic scaffolding protein PSD-95 opposite vGluT2-labeled boutons from the SI (Henny and Jones, 2006a). We now show that about 80% of the orexin neurons are innervated by glutamatergic SI boutons, and about 80% of the orexin neurons respond to optogenetic stimulation of glutamatergic SI terminals.

Most research on the BF has focused on the cholinergic and GABAergic neurons, but much less is known about the functions of the glutamatergic BF neurons. Hassani and colleagues used extracellular recordings with juxtacellular labeling to study putative glutamatergic BF neurons in vivo, and found that these neurons are mainly active during wakefulness and REM sleep (Hassani et al., 2009). Specifically, these non-cholinergic, non-GABAergic neurons primarily fire in association with fast cortical rhythms, though a few may be more active during NREM sleep. A recent study (Xu et al., 2015) using optrode recordings in reporter mice confirms that these vGluT2+ BF cells primarily fire during wake and REM sleep, and are less active during NREM sleep, and optogenetic activation of these neurons induced a rapid transition from NREM sleep to wakefulness.

The orexin neurons are clearly active during wake. In rodents, FOS studies plus juxtacellular and unit recordings show that orexin neurons are mostly active during wakefulness (Estabrooke et al., 2001; Mileykovskiy et al., 2005; Lee et al., 2005), and in humans, extracellular levels of orexin-A can be six times higher during wake than during sleep (Blouin et al., 2013). In cats, brain and CSF orexin peptide concentrations are increased during wake (Kiyashchenko et al., 2002). Furthermore, NMDA administration in the LH increases wakefulness in wild-type (WT) mice but less so in orexin knock-out mice (Kostin et al., 2014). Last, prolonged wakefulness and food deprivation increase EPSCs on orexin neurons (Horvath and Gao, 2005; Rao et al., 2007).

Most likely, glutamatergic BF neurons and orexin neurons excite each other during wake, and this positive feedback promotes arousal. Additionally, both the BF and orexin neurons have been implicated in motivated behaviors. As adequate arousal is required for all motivated behaviors, this circuit may promote both arousal and motivation.

Possible functions of the GABAergic BF projection

With bright field and fluorescence microscopy, GABAergic BF neurons formed numerous apparent synapses on orexin neurons, but CRACM showed few direct responses. This was unexpected as these GABAergic boutons contain synaptophysin presynaptically, and Henny and Jones (2006) demonstrated that in rats, orexin neurons express the postsynaptic scaffolding protein gephyrin opposite boutons from BF GABAergic neurons, suggesting the

presence of functional synapses. In addition, GABA can inhibit the orexin neurons (Yamanaka et al., 2003; Xie et al., 2006), and photostimulation of GABAergic fibers from the POA rapidly inhibits the orexin neurons (Saito et al., 2013). Most importantly, the CRACM method was clearly effective as it elicited GABA release from SI terminals and short latency IPSPs on adjacent non-orexin neurons. Sleep deprivation can increase the expression of GABAA receptors on orexin neurons (Toosi et al., 2016), and it is possible that CRACM would show stronger connectivity after sleep deprivation.

Researchers have long appreciated that light microscopy can suggest false positive synaptic connectivity. For example, Meredith and Wouterlood found that hippocampal projections formed apparent appositions on cholinergic neurons in the nucleus accumbens when studied with light microscopy, but they could not detect any synaptic contacts with electron microscopy (Meredith and Wouterlood, 1990). Instead, the hippocampal projections synapsed on adjacent, non-cholinergic neurons. Similarly, it seems most likely that the GABAergic terminals from the SI synapse on non-orexin LH neurons. In ongoing research, we are now examining whether these non-orexin neurons form a local circuit through which they influence the orexin neurons.

BF GABAergic neurons are functionally heterogeneous, and these populations may have distinct effects on the orexin and other LH neurons. GABAergic BF neurons can differ in their expression of peptides such as parvalbumin, calbindin, and somatostatin (Gritti et al., 2003; Xu et al., 2015), basic membrane properties (McKenna et al., 2013), and in vivo firing patterns (Hassani et al., 2009). Hassani and colleagues showed that most GABAergic neurons in the SI and MCPO fire during wake and/or REM sleep, but 28% fire mainly during NREM sleep (Hassani et al., 2009). Cortically-projecting GABAergic neurons likely fire in association with fast EEG frequencies (Kim et al., 2015; Manns et al., 2000). Xu and colleagues (Xu et al., 2015) showed that optogenetic stimulation of parvalbumin and somatostatin BF neurons caused a significant increase in wakefulness and NREM sleep, respectively, but which types of GABAergic neurons innervate the LH remains unknown. Unilateral inhibition of the BF can induce Fos in ipsilateral orexin neurons, suggesting that some BF neurons inhibit the orexin neurons (Satoh et al., 2003), but a wake-active GABAergic projection onto the orexin neurons seems counterproductive for wake maintenance. Therefore, wake-active GABAergic neurons probably do not directly innervate the orexin neurons, but they may indirectly excite the orexin neurons via an inhibitory LH interneuron. Clearly, more work is needed to define the anatomy and functions of these large, descending GABAergic projections.

Limitations

One potential limitation of our experiments is that we focused on glutamatergic signaling mediated by neurons containing vGluT2. Most glutamatergic BF neurons contain vGluT2, but a subset of ChAT and potentially parvalbumin-containing BF neurons contain vGlut3 (Harkany et al., 2003; Nickerson Poulin et al., 2006; Gritti et al., 2006). Thus, it is possible that some cholinergic BF neurons co-release glutamate as has been shown in cholinergic interneurons in the striatum (Higley et al., 2011). However, this is unlikely to be a glutamatergic influence on the orexin neurons as cholinergic BF neurons do not innervate

the orexin neurons in mice. In addition, we have seen no evidence of glutamate release from GABAergic BF neurons using optogenetics (these experiments and unpublished results).

Research on the SI is confounded by definitions that differ between research groups. Nomenclature to describe or subdivide this region includes the SI, ventral pallidum (VP), extended amydgala, nucleus basalis, and IPAC. While some refer to this entire region as the SI (Canteras et al., 1995), others propose that VP and extended amygdala are rostral and caudal divisions of the SI (Alheid, 2003; Heimer et al., 1997). In part, this complexity arises from differences in BF anatomy across species as cholinergic groups form tighter clusters and are defined differently in primates than in rodents. We operationally define the SI as the loosely packed subcommissural group of neurons within the boundary of magnocellular cholinergic neurons that are located dorsal to the more densely packed MCPO and HDB, and ventral/medial to the GP (Figure 3). The basal nucleus, ventral pallidum, and extended amygdala, as described by others may overlap with the region we define as SI or they may be distinct subregions. We appreciate the complexity of the nomenclature and the difficulty of categorizing the neurons in this area, and hopefully, future research will identify specific neuronal markers to better define the SI, especially in relation to the VP and extended amygdala.

Another limitation is the challenge of tracing pathways in the small brains of mice. We injected very small (3 nl) volumes of AAV-ChR2-mCherry, but injections occasionally spread into adjacent parts of the BF. We managed this problem by limiting our analysis to injections confined to specific BF regions and within cholinergic boundaries, as is typical with many anatomical studies. Conversely, because our injections were small, our analyses may underestimate of the density of the projections from a given BF structure.

Finally, several factors could affect the accuracy of counting appositions with light microscopy. We counted BF appositions only at the soma and proximal dendrites of orexin neurons, as it is challenging to analyze appositions onto distal dendrites. Conversely, though we counted only appositions that appeared immediately adjacent to the orexin neurons, we may have over-counted appositions that actually contacted nearby structures such as another neuron or presynaptic terminals. In addition, dehydration and shrinkage of sections could have made boutons and orexin neurons appear closer. Regardless of the precision in counting appositions, light microscopy is only a start for identifying potential synapses, and the presence of true synapses needs to be established using electron microscopy or electrophysiology.

Conclusions

Glutamatergic and GABAergic neurons of the SI and MCPO send dense projections to the orexin neurons, and the glutamatergic synapses excite the orexin neurons while the GABA synapses appear to have weak direct connectivity (Figure 8). Considering the intensity of these projections, the BF and orexin neurons likely work in concert to promote arousal, motivation, and other behaviors.

Acknowledgments

Support: NIH grants P01 HL095491, P01 HL095491-02S1, R21 NS082854, and T32 AG000222.

We appreciate much thoughtful feedback on anatomy from Dr. Clif Saper. We thank Dr. Patrick Fuller for giving us the AAV-ChR2-YFP, and Dr. Takeshi Sakurai for his kind gift of the AAV construct for the AAV8-horexin-tdTomato.

Abbreviations

3V	third ventricle
AAV	adeno-associated viral vector
ac	anterior commissure
Acb	accumbens nucleus
Arc	arcuate hypothalamic nucleus
BDA	biotinylated dextran amines
BF	basal forebrain
BLA	basolateral amygdala
CEL	central amygdala nucleus, lateral
ChAT	choline acetyltransferase
ChR2	Channelrhodopsin-2
CPu	caudate putamen
CRACM	Channelrhodopsin-Assisted Circuit Mapping
DAB	diaminobenzidine
DMH	dorsomedial hypothalamic nucleus
GP	globus pallidus
HDB	horizontal nucleus of the diagonal band
ic	internal capsule
ip	intraperitoneal
f	fornix
LH	lateral hypothalamus
LHp	posterior lateral hypothalamus
LSD	lateral septum, dorsal
LSI	lateral septum, intermediate

LPO	lateral preoptic area
MCPO	magnocellular preoptic nucleus
mfb	medial forebrain bundle
MPA	medial preoptic area
MPO	medial preoptic nucleus
MS	medial septum
och	optic chiasm
opt	optic tract
Ox	orexin neurons
PVH	paraventricular nucleus
PeF	perifornical nucleus of the hypothalamus
SCh	suprachiasmatic nucleus
SI	substantia innominata
st	stria terminalis
VDB	vertical nucleus of the diagonal band
vGAT	vesicular GABA transporter
vGluT1	vesicular glutamate transporter, type 1
vGluT2	vesicular glutamate transporter, type 2
vGluT3	vesicular glutamate transporter, type 3
VMH	ventromedial nucleus of the hypothalamus
VP	ventral pallidum
YFP	yellow fluorescent protein

Literature Cited

Adamantidis A, Carter MC, de Lecea L. Optogenetic deconstruction of sleep-wake circuitry in the brain. Front Mol Neurosci. 2010; 2:31. [PubMed: 20126433]

Alheid GF. Extended amygdala and basal forebrain. Ann N Y Acad Sci. 2003; 985:185–205. [PubMed: 12724159]

Arrigoni E, Mochizuki T, Scammell TE. Activation of the basal forebrain by the orexin/hypocretin neurones. Acta Physiol (Oxf). 2010; 198(3):223–235. [PubMed: 19723027]

Bayer L, Eggermann E, Serafin M, Grivel J, Machard D, Muhlethaler M, Jones BE. Opposite effects of noradrenaline and acetylcholine upon hypocretin/orexin versus melanin concentrating hormone neurons in rat hypothalamic slices. Neuroscience. 2005; 130(4):807–811. [PubMed: 15652980]

Blanco-Centurion CA, Shiromani A, Winston E, Shiromani PJ. Effects of hypocretin-1 in 192-IgG-saporin-lesioned rats. Eur J Neurosci. 2006; 24(7):2084–2088. [PubMed: 17067305]

Blouin AM, Fried I, Wilson CL, Staba RJ, Behnke EJ, Lam HA, Maidment NT, Karlsson KAE, Lapierre JL, Siegel JM. Human hypocretin and melanin-concentrating hormone levels are linked to emotion and social interaction. Nat Commun. 2013; 4:1547. [PubMed: 23462990]

Brashear HR, Zaborszky L, Heimer L. Distribution of GABAergic and cholinergic neurons in the rat diagonal band. Neuroscience. 1986; 17(2):439–451. [PubMed: 3517690]

Canteras NS, Simerly RB, Swanson LW. Organization of projections from the medial nucleus of the amygdala: a PHAL study in the rat. J Comp Neurol. 1995; 360(2):213–245. [PubMed: 8522644]

Chemelli RM, Willie JT, Sinton CM, Elmquist JK, Scammell T, Lee C, Richardson JA, Williams SC, Xiong Y, Kisanuki Y, Fitch TE, Nakazato M, Hammer RE, Saper CB, Yanagisawa M. Narcolepsy in orexin knockout mice: molecular genetics of sleep regulation. Cell. 1999; 98(4):437–451. [PubMed: 10481909]

Chen MC, Ferrari L, Sacchet MD, Foland-Ross LC, Qiu MH, Gotlib IH, Fuller PM, Arrigoni E, Lu J. Identification of a direct GABAergic pallidocortical pathway in rodents. Eur J Neurosci. 2015; 41(6):748–759. [PubMed: 25581560]

Dinopoulos A, Parnavelas JG, Eckenstein F. Morphological characterization of cholinergic neurons in the horizontal limb of the diagonal band of Broca in the basal forebrain of the rat. J Neurocytol. 1986; 15(5):619–628. [PubMed: 3534149]

Eggermann E, Serafin M, Bayer L, Machard D, Saint-Mleux B, Jones BE, Muhlethaler M. Orexins/hypocretins excite basal forebrain cholinergic neurones. Neuroscience. 2001; 108(2):177–181. [PubMed: 11734353]

España RA, Baldo BA, Kelley AE, Berridge CW. Wake-promoting and sleep-suppressing actions of hypocretin (orexin): basal forebrain sites of action. Neuroscience. 2001; 106(4):699–715. [PubMed: 11682157]

España RA, Reis KM, Valentino RJ, Berridge CW. Organization of hypocretin/orexin efferents to locus coeruleus and basal forebrain arousal-related structures. J Comp Neurol. 2005; 481(2):160–178. [PubMed: 15562511]

Estabrooke IV, McCarthy MT, Ko E, Chou TC, Chemelli RM, Yanagisawa M, Saper CB, Scammell TE. Fos expression in orexin neurons varies with behavioral state. J Neurosci. 2001; 21(5):1656–1662. [PubMed: 11222656]

Everitt BJ, Robbins TW. Central cholinergic systems and cognition. Annu Rev Psychol. 1997; 48:649–684. [PubMed: 9046571]

Fadel J, Bubser M, Deutch AY. Differential activation of orexin neurons by antipsychotic drugs associated with weight gain. J Neurosci. 2002; 22(15):6742–6746. [PubMed: 12151553]

Fadel J, Frederick-Duus D. Orexin/hypocretin modulation of the basal forebrain cholinergic system: insights from in vivo microdialysis studies. Pharmacol Biochem Behav. 2008; 90(2):156–162. [PubMed: 18281084]

Franklin, KB., Paxinos, G. The Mouse Brain in Stereotaxic Coordinates. Third. New York, New York: Elsevier; 2007.

Fuller PM, Sherman D, Pedersen NP, Saper CB, Lu J. Reassessment of the structural basis of the ascending arousal system. J Comp Neurol. 2011; 519(5):933–956. [PubMed: 21280045]

Garfield AS, Shah BP, Madara JC, Burke LK, Patterson CM, Flak J, Neve RL, Evans ML, Lowell BB, Myers MG Jr, Heisler LK. A parabrachial-hypothalamic cholecystokinin neurocircuit controls counterregulatory responses to hypoglycemia. Cell Metab. 2014; 20(6):1030–1037. [PubMed: 25470549]

Gautron L, Lazarus M, Scott MM, Saper CB, Elmquist JK. Identifying the efferent projections of leptin-responsive neurons in the dorsomedial hypothalamus using a novel conditional tracing approach. J Comp Neurol. 2010; 518(11):2090–2108. [PubMed: 20394060]

Goard M, Dan Y. Basal forebrain activation enhances cortical coding of natural scenes. Nat Neurosci. 2009; 12(11):1444–1449. [PubMed: 19801988]

Gritti I, Henny P, Galloni F, Mainville L, Mariotti M, Jones BE. Stereological estimates of the basal forebrain cell population in the rat, including neurons containing choline acetyltransferase,

glutamic acid decarboxylase or phosphate-activated glutaminase and colocalizing vesicular glutamate transporters. Neuroscience. 2006; 143(4):1051–1064. [PubMed: 17084984]

Gritti I, Mainville L, Jones BE. Projections of GABAergic and cholinergic basal forebrain and GABAergic preoptic-anterior hypothalamic neurons to the posterior lateral hypothalamus of the rat. J Comp Neurol. 1994; 339(2):251–268. [PubMed: 8300907]

Gritti I, Mainville L, Mancia M, Jones BE. GABAergic and other noncholinergic basal forebrain neurons, together with cholinergic neurons, project to the mesocortex and isocortex in the rat. J Comp Neurol. 1997; 383(2):163–177. [PubMed: 9182846]

Gritti I, Manns ID, Mainville L, Jones BE. Parvalbumin, calbindin, or calretinin in cortically projecting and GABAergic, cholinergic, or glutamatergic basal forebrain neurons of the rat. J Comp Neurol. 2003; 458(1):11–31. [PubMed: 12577320]

Grove EA. Efferent connections of the substantia innominata in the rat. J Comp Neurol. 1988; 277(3): 347–364. [PubMed: 2461973]

Hallanger AE, Wainer BH. Ascending projections from the pedunculopontine tegmental nucleus and the adjacent mesopontine tegmentum in the rat. J Comp Neurol. 1988; 274(4):483–515. [PubMed: 2464621]

Han Y, Shi YF, Xi W, Zhou R, Tan ZB, Wang H, Li XM, Chen Z, Feng G, Luo M, Huang ZL, Duan S, Yu YQ. Selective activation of cholinergic basal forebrain neurons induces immediate sleep-wake transitions. Curr Biol. 2014; 24(6):693–698. [PubMed: 24613308]

Harkany T, Hartig W, Berghuis P, Dobszay MB, Zilberter Y, Edwards RH, Mackie K, Ernfors P. Complementary distribution of type 1 cannabinoid receptors and vesicular glutamate transporter 3 in basal forebrain suggests input-specific retrograde signalling by cholinergic neurons. Eur J Neurosci. 2003; 18(7):1979–1992. [PubMed: 14622230]

Harris GC, Aston-Jones G. Arousal and reward: a dichotomy in orexin function. Trends Neurosci. 2006; 29(10):571–577. [PubMed: 16904760]

Harris GC, Wimmer M, Aston-Jones G. A role for lateral hypothalamic orexin neurons in reward seeking. Nature. 2005; 437(7058):556–559. [PubMed: 16100511]

Hassani OK, Lee MG, Henny P, Jones BE. Discharge profiles of identified GABAergic in comparison to cholinergic and putative glutamatergic basal forebrain neurons across the sleep-wake cycle. J Neurosci. 2009; 29(38):11828–11840. [PubMed: 19776269]

Hedreen JC, Struble RG, Whitehouse PJ, Price DL. Topography of the magnocellular basal forebrain system in human brain. J Neuropathol Exp Neurol. 1984; 43(1):1–21. [PubMed: 6319616]

Heimer L, Harlan RE, Alheid GF, Garcia MM, de Olmos J. Substantia innominata: a notion which impedes clinical-anatomical correlations in neuropsychiatric disorders. Neuroscience. 1997; 76(4): 957–1006. [PubMed: 9027863]

Henny P, Jones BE. Innervation of orexin/hypocretin neurons by GABAergic, glutamatergic or cholinergic basal forebrain terminals evidenced by immunostaining for presynaptic vesicular transporter and postsynaptic scaffolding proteins. J Comp Neurol. 2006a; 499(4):645–661. [PubMed: 17029265]

Henny P, Jones BE. Vesicular glutamate (VGlut), GABA (VGAT), and acetylcholine (VACht) transporters in basal forebrain axon terminals innervating the lateral hypothalamus. J Comp Neurol. 2006b; 496(4):453–467. [PubMed: 16572456]

Higley MJ, Gittis AH, Oldenburg IA, Balthasar N, Seal RP, Edwards RH, Lowell BB, Kreitzer AC, Sabatini BL. Cholinergic interneurons mediate fast VGluT3-dependent glutamatergic transmission in the striatum. PLoS One. 2011; 6(4):e19155. [PubMed: 21544206]

Horvath TL, Gao XB. Input organization and plasticity of hypocretin neurons: possible clues to obesity's association with insomnia. Cell Metab. 2005; 1(4):279–286. [PubMed: 16054072]

Hull C, Adesnik H, Scanziani M. Neocortical disynaptic inhibition requires somatodendritic integration in interneurons. J Neurosci. 2009; 29(28):8991–8995. [PubMed: 19605636]

Hur EE, Zaborszky L. Vglut2 afferents to the medial prefrontal and primary somatosensory cortices: a combined retrograde tracing in situ hybridization study [corrected]. J Comp Neurol. 2005; 483(3): 351–373. [PubMed: 15682395]

Irmak SO, de Lecea L. Basal forebrain cholinergic modulation of sleep transitions. Sleep. 2014; 37(12):1941–1951. [PubMed: 25325504]

Isaac JT, Nicoll RA, Malenka RC. Evidence for silent synapses: implications for the expression of LTP. Neuron. 1995; 15(2):427–434. [PubMed: 7646894]

Jones BE. Activity, modulation and role of basal forebrain cholinergic neurons innervating the cerebral cortex. Prog Brain Res. 2004; 145:157–169. [PubMed: 14650914]

Jones BE. Modulation of cortical activation and behavioral arousal by cholinergic and orexinergic systems. Ann N Y Acad Sci. 2008; 1129:26–34. [PubMed: 18591466]

Kim T, Thankachan S, McKenna JT, McNally JM, Yang C, Choi JH, Chen L, Kocsis B, Deisseroth K, Strecker RE, Basheer R, Brown RE, McCarley RW. Cortically projecting basal forebrain parvalbumin neurons regulate cortical gamma band oscillations. Proc Natl Acad Sci U S A. 2015; 112(11):3535–3540. [PubMed: 25733878]

Kiyashchenko LI, Mileykovskiy BY, Maidment N, Lam HA, Wu MF, John J, Peever J, Siegel JM. Release of hypocretin (orexin) during waking and sleep states. J Neurosci. 2002; 22(13):5282–5286. [PubMed: 12097478]

Kostin A, Siegel JM, Alam MN. Lack of hypocretin attenuates behavioral changes produced by glutamatergic activation of the perifornical-lateral hypothalamic area. Sleep. 2014; 37(5):1011–1020. [PubMed: 24790280]

Lee MG, Hassani OK, Jones BE. Discharge of identified orexin/hypocretin neurons across the sleep-waking cycle. J Neurosci. 2005; 25(28):6716–6720. [PubMed: 16014733]

Liao D, Hessler NA, Malinow R. Activation of postsynaptically silent synapses during pairing-induced LTP in CA1 region of hippocampal slice. Nature. 1995; 375(6530):400–404. [PubMed: 7760933]

Lin SC, Nicolelis MA. Neuronal ensemble bursting in the basal forebrain encodes salience irrespective of valence. Neuron. 2008; 59(1):138–149. [PubMed: 18614035]

Ljubojevic V, Luu P, De Rosa E. Cholinergic contributions to supramodal attentional processes in rats. J Neurosci. 2014; 34(6):2264–2275. [PubMed: 24501365]

Manns ID, Alonso A, Jones BE. Discharge profiles of juxtacellularly labeled and immunohistochemically identified GABAergic basal forebrain neurons recorded in association with the electroencephalogram in anesthetized rats. J Neurosci. 2000; 20(24):9252–9263. [PubMed: 11125003]

Marcus JN, Aschkenasi CJ, Lee CE, Chemelli RM, Saper CB, Yanagisawa M, Elmquist JK. Differential expression of orexin receptors 1 and 2 in the rat brain. J Comp Neurol. 2001; 435(1): 6–25. [PubMed: 11370008]

Matsuki T, Takasu M, Hirose Y, Murakoshi N, Sinton CM, Motoike T, Yanagisawa M. GABAA receptor-mediated input change on orexin neurons following sleep deprivation in mice. Neuroscience. 2015; 284:217–224. [PubMed: 25286384]

McKenna JT, Yang C, Franciosi S, Winston S, Abarr KK, Rigby MS, Yanagawa Y, McCarley RW, Brown RE. Distribution and intrinsic membrane properties of basal forebrain GABAergic and parvalbumin neurons in the mouse. J Comp Neurol. 2013; 521(6):1225–1250. [PubMed: 23254904]

Meredith GE, Wouterlood FG. Hippocampal and midline thalamic fibers and terminals in relation to the choline acetyltransferase-immunoreactive neurons in nucleus accumbens of the rat: a light and electron microscopic study. J Comp Neurol. 1990; 296(2):204–221. [PubMed: 2358532]

Mileykovskiy BY, Kiyashchenko LI, Siegel JM. Behavioral correlates of activity in identified hypocretin/orexin neurons. Neuron. 2005; 46(5):787–798. [PubMed: 15924864]

Nickerson Poulin A, Guerci A, El Mestikawy S, Semba K. Vesicular glutamate transporter 3 immunoreactivity is present in cholinergic basal forebrain neurons projecting to the basolateral amygdala in rat. J Comp Neurol. 2006; 498(5):690–711. [PubMed: 16917846]

Ohno K, Hondo M, Sakurai T. Cholinergic regulation of orexin/hypocretin neurons through M(3) muscarinic receptor in mice. J Pharmacol Sci. 2008; 106(3):485–491. [PubMed: 18344611]

Peyron C, Faraco J, Rogers W, Ripley B, Overeem S, Charnay Y, Nevsimalova S, Aldrich M, Reynolds D, Albin R, Li R, Hungs M, Pedrazzoli M, Padigaru M, Kucherlapati M, Fan J, Maki R, Lammers GJ, Bouras C, Kucherlapati R, Nishino S, Mignot E. A mutation in a case of early onset narcolepsy and a generalized absence of hypocretin peptides in human narcoleptic brains. Nature Medicine. 2000; 6(9):991–997.

Peyron C, Tighe DK, van den Pol AN, de Lecea L, Heller HC, Sutcliffe JG, Kilduff TS. Neurons containing hypocretin (orexin) project to multiple neuronal systems. J Neurosci. 1998; 18(23): 9996–10015. [PubMed: 9822755]

Pinto L, Goard MJ, Estandian D, Xu M, Kwan AC, Lee SH, Harrison TC, Feng G, Dan Y. Fast modulation of visual perception by basal forebrain cholinergic neurons. Nat Neurosci. 2013; 16(12):1857–1863. [PubMed: 24162654]

Rao Y, Liu ZW, Borok E, Rabenstein RL, Shanabrough M, Lu M, Picciotto MR, Horvath TL, Gao XB. Prolonged wakefulness induces experience-dependent synaptic plasticity in mouse hypocretin/orexin neurons. J Clin Invest. 2007; 117(12):4022–4033. [PubMed: 18060037]

Raver SM, Lin SC. Basal forebrain motivational salience signal enhances cortical processing and decision speed. Front Behav Neurosci. 2015; 9:277. [PubMed: 26528157]

Rizzoli SO. Synaptic vesicle recycling: steps and principles. EMBO J. 2014; 33(8):788–822. [PubMed: 24596248]

Rossi J, Balthasar N, Olson D, Scott M, Berglund E, Lee CE, Choi MJ, Lauzon D, Lowell BB, Elmquist JK. Melanocortin-4 receptors expressed by cholinergic neurons regulate energy balance and glucose homeostasis. Cell Metab. 2011; 13(2):195–204. [PubMed: 21284986]

Rye DB, Wainer BH, Mesulam MM, Mufson EJ, Saper CB. Cortical projections arising from the basal forebrain: a study of cholinergic and noncholinergic components employing combined retrograde tracing and immunohistochemical localization of choline acetyltransferase. Neuroscience. 1984; 13(3):627–643. [PubMed: 6527769]

Saito YC, Tsujino N, Hasegawa E, Akashi K, Abe M, Mieda M, Sakimura K, Sakurai T. GABAergic neurons in the preoptic area send direct inhibitory projections to orexin neurons. Front Neural Circuits. 2013; 7:192. [PubMed: 24348342]

Sakurai T, Nagata R, Yamanaka A, Kawamura H, Tsujino N, Muraki Y, Kageyama H, Kunita S, Takahashi S, Goto K, Koyama Y, Shioda S, Yanagisawa M. Input of orexin/hypocretin neurons revealed by a genetically encoded tracer in mice. Neuron. 2005; 46(2):297–308. [PubMed: 15848807]

Saper CB. Organization of cerebral cortical afferent systems in the rat. II. Magnocellular basal nucleus. J Comp Neurol. 1984; 222(3):313–342. [PubMed: 6699210]

Saper CB, Fuller PM, Pedersen NP, Lu J, Scammell TE. Sleep state switching. Neuron. 2010; 68(6): 1023–1042. [PubMed: 21172606]

Sarter M, Hasselmo ME, Bruno JP, Givens B. Unraveling the attentional functions of cortical cholinergic inputs: interactions between signal-driven and cognitive modulation of signal detection. Brain Res Brain Res Rev. 2005; 48(1):98–111. [PubMed: 15708630]

Satoh K, Fibiger HC. Cholinergic neurons of the laterodorsal tegmental nucleus: efferent and afferent connections. J Comp Neurol. 1986; 253(3):277–302. [PubMed: 2432101]

Satoh S, Matsumura H, Nakajima T, Nakahama K, Kanbayashi T, Nishino S, Yoneda H, Shigeyoshi Y. Inhibition of rostral basal forebrain neurons promotes wakefulness and induces FOS in orexin neurons. Eur J Neurosci. 2003; 17(8):1635–1645. [PubMed: 12752381]

Schone C, Venner A, Knowles D, Karnani MM, Burdakov D. Dichotomous cellular properties of mouse orexin/hypocretin neurons. J Physiol. 2011; 589(Pt 11):2767–2779. [PubMed: 21486780]

Schwaber JS, Rogers WT, Satoh K, Fibiger HC. Distribution and organization of cholinergic neurons in the rat forebrain demonstrated by computer-aided data acquisition and three-dimensional reconstruction. J Comp Neurol. 1987; 263(3):309–325. [PubMed: 2822773]

Semba K. Multiple output pathways of the basal forebrain: organization, chemical heterogeneity, and roles in vigilance. Behav Brain Res. 2000; 115(2):117–141. [PubMed: 11000416]

Semba K, Reiner PB, McGeer EG, Fibiger HC. Brainstem afferents to the magnocellular basal forebrain studied by axonal transport, immunohistochemistry, and electrophysiology in the rat. J Comp Neurol. 1988; 267(3):433–453. [PubMed: 2449477]

Shi YF, Han Y, Su YT, Yang JH, Yu YQ. Silencing of Cholinergic Basal Forebrain Neurons Using Archaerhodopsin Prolongs Slow-Wave Sleep in Mice. PLoS One. 2015; 10(7):e0130130. [PubMed: 26151909]

Swanson LW. Cerebral hemisphere regulation of motivated behavior. Brain Res. 2000; 886(1–2):113–164. [PubMed: 11119693]

Swanson LW, Mogenson GJ, Gerfen CR, Robinson P. Evidence for a projection from the lateral preoptic area and substantia innominata to the 'mesencephalic locomotor region' in the rat. Brain Res. 1984; 295(1):161–178. [PubMed: 6201228]

Tasker JG, Oliet SH, Bains JS, Brown CH, Stern JE. Glial regulation of neuronal function: from synapse to systems physiology. J Neuroendocrinol. 2012; 24(4):566–576. [PubMed: 22128866]

Thakkar MM, Ramesh V, Strecker RE, McCarley RW. Microdialysis perfusion of orexin-A in the basal forebrain increases wakefulness in freely behaving rats. Arch Ital Biol. 2001; 139(3):313–328. [PubMed: 11330208]

Thannickal TC, Moore RY, Nienhuis R, Ramanathan L, Gulyani S, Aldrich M, Cornford M, Siegel JM. Reduced number of hypocretin neurons in human narcolepsy. Neuron. 2000; 27(3):469–474. [PubMed: 11055430]

Theodosis DT, Montagnese C, Rodriguez F, Vincent JD, Poulain DA. Oxytocin induces morphological plasticity in the adult hypothalamo-neurohypophysial system. Nature. 1986; 322(6081):738–740. [PubMed: 3748154]

Theodosis DT, Poulain DA. Evidence for structural plasticity in the supraoptic nucleus of the rat hypothalamus in relation to gestation and lactation. Neuroscience. 1984; 11(1):183–193. [PubMed: 6709185]

Theodosis DT, Poulain DA, Vincent JD. Possible morphological bases for synchronisation of neuronal firing in the rat supraoptic nucleus during lactation. Neuroscience. 1981; 6(5):919–929. [PubMed: 7242921]

Toossi H, Del Cid-Pellitero E, Jones BE. GABA Receptors on Orexin and Melanin-Concentrating Hormone Neurons Are Differentially Homeostatically Regulated Following Sleep Deprivation. eNeuro. 2016; 3(3)

Tweedle CD, Hatton GI. Ultrastructural changes in rat hypothalamic neurosecretory cells and their associated glia during minimal dehydration and rehydration. Cell Tissue Res. 1977; 181(1):59–72. [PubMed: 880623]

Vong L, Ye C, Yang Z, Choi B, Chua S Jr, Lowell BB. Leptin action on GABAergic neurons prevents obesity and reduces inhibitory tone to POMC neurons. Neuron. 2011; 71(1):142–154. [PubMed: 21745644]

Voytko ML, Olton DS, Richardson RT, Gorman LK, Tobin JR, Price DL. Basal forebrain lesions in monkeys disrupt attention but not learning and memory. J Neurosci. 1994; 14(1):167–186. [PubMed: 8283232]

Wu M, Zaborszky L, Hajszan T, van den Pol A, Alreja M. Hypocretin/orexin innervation and excitation of identified septohippocampal cholinergic neurons. J Neurosci. 2004; 24(14):3527–3536. [PubMed: 15071100]

Xie X, Crowder TL, Yamanaka A, Morairty SR, Lewinter RD, Sakurai T, Kilduff TS. GABA(B) receptor-mediated modulation of hypocretin/orexin neurones in mouse hypothalamus. J Physiol. 2006; 574(Pt 2):399–414. [PubMed: 16627567]

Xu M, Chung S, Zhang S, Zhong P, Ma C, Chang WC, Weissbourd B, Sakai N, Luo L, Nishino S, Dan Y. Basal forebrain circuit for sleep-wake control. Nat Neurosci. 2015

Yamanaka A, Muraki Y, Tsujino N, Goto K, Sakurai T. Regulation of orexin neurons by the monoaminergic and cholinergic systems. Biochem Biophys Res Commun. 2003; 303(1):120–129. [PubMed: 12646175]

Yoshida K, McCormack S, Espana RA, Crocker A, Scammell TE. Afferents to the orexin neurons of the rat brain. J Comp Neurol. 2006; 494(5):845–861. [PubMed: 16374809]

Zaborszky L, Duque A. Sleep-wake mechanisms and basal forebrain circuitry. Front Biosci. 2003; 8:d1146–1169. [PubMed: 12957822]

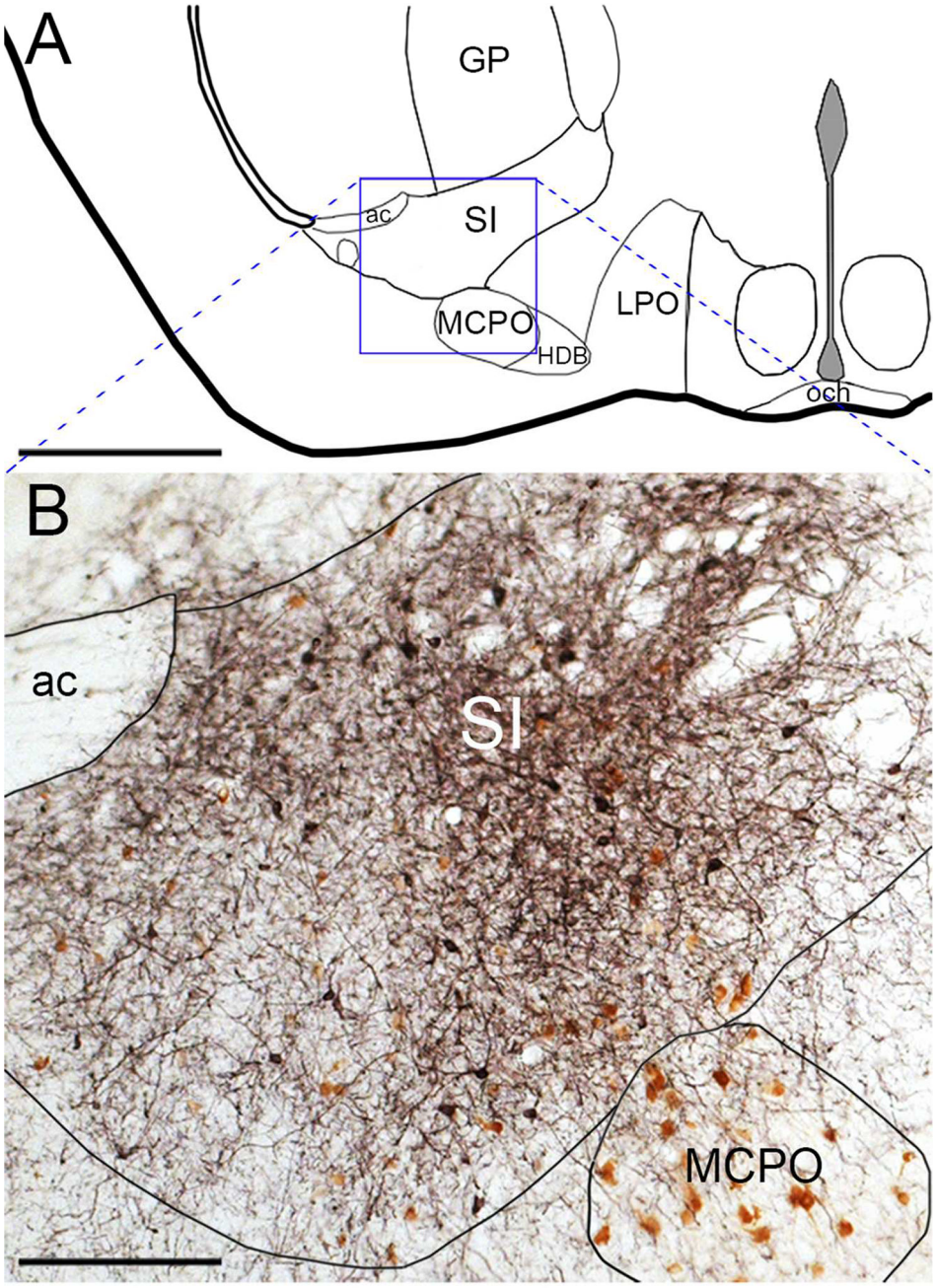

Figure 1. A typical AAV-ChR2 injection site in the SI

(A) Diagram of the SI/MCPO region. **(B)** DsRed antisera (black) robustly labels ChR2-mCherry fusion protein in neuronal soma and axons of a vGAT-Cre mouse. DAB (brown) labels ChAT neurons in the SI and MCPO. Scale bars are 1 mm in A and 200 μm in B.

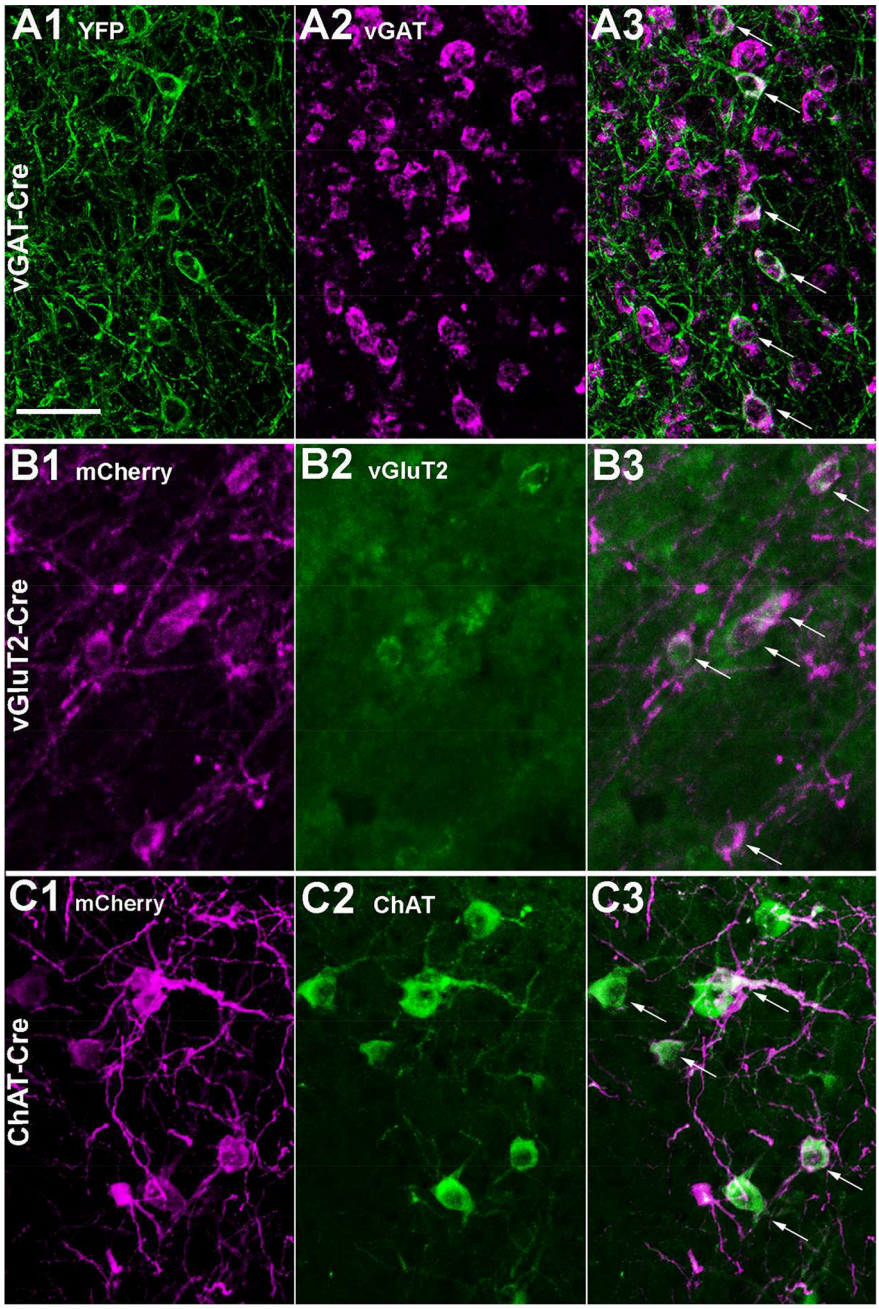

Figure 2. Selective expression of marker proteins in SI neuronal populations

(A1) In a vGAT-cre mouse, injection of AAV-ChR2-YFP results in robust GFP immunoreactivity in neurons of the SI. **(A2–A3)** In situ hybridization for vGAT mRNA and merged image; arrows mark double labeled soma. **(B1)** In a vGluT2-Cre mouse, injection of AAV-ChR2-mCherry produces strong mCherry labeling. (**B2–B3)** vGluT2 mRNA and merged image. (**C)** In a ChAT-Cre mouse, injection of AAV-ChR2-mCherry produces strong mCherry labeling. **(C1–C2)** Immunolabeling for ChAT and merged image. Scale bar is 50 μm.

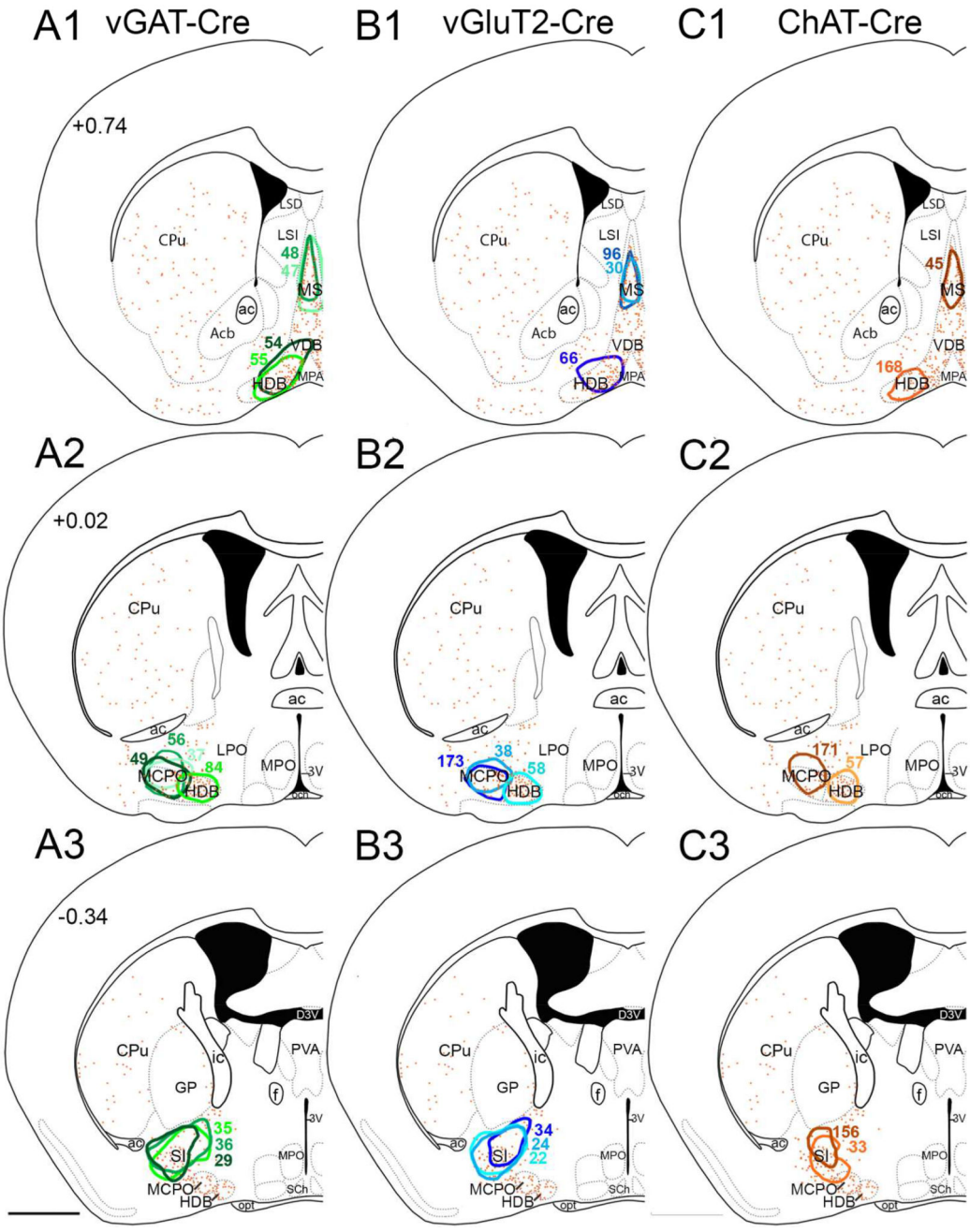

Figure 3. Distribution of injection sites

(A1–A3) BF injection sites from vGAT-Cre mice, **(B1–B3)** vGluT2-Cre mice, and **(C1–C3)** ChAT-Cre mice. Colored outlines show the center of each injection site. Orange dots show the distribution of cholinergic neurons, and atlas levels are per Franklin and Paxinos, 2007. Scale bar is 1 mm.

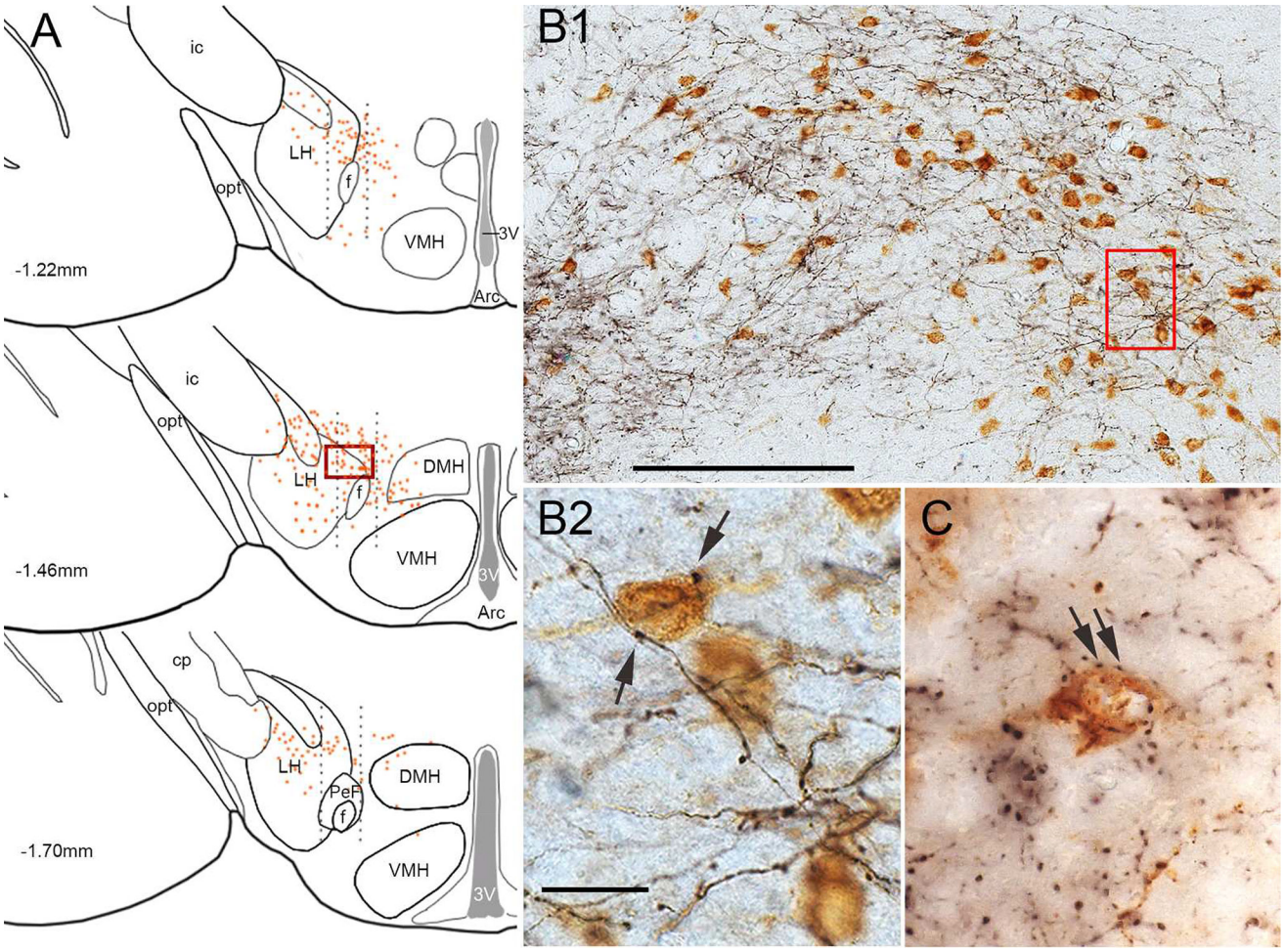

Figure 4. SI innervation of the orexin neurons

(A) We analyzed three sections (spaced 240 μm apart) through the rostral-caudal extent of the orexin field. Dotted black lines indicate the lateral, perifornical, and medial divisions of the orexin field; orange dots represent individual orexin neurons. **(B1)** Higher power image of the boxed area in A shows that mCherry-labeled glutamatergic axons (black) are dense within the orexin field, and **(B2)** Higher power image of the boxed area in B1 shows that mCherry-labeled boutons (arrows) closely appose orexin neurons (brown). **(C)** After injection of AAV-synaptophysin-mCherry, mCherry-labeled, GABAergic presynaptic terminals (black) closely appose orexin neurons (brown). Scale bars in B1 and B2 are 200 μm and 25 μm, respectively.

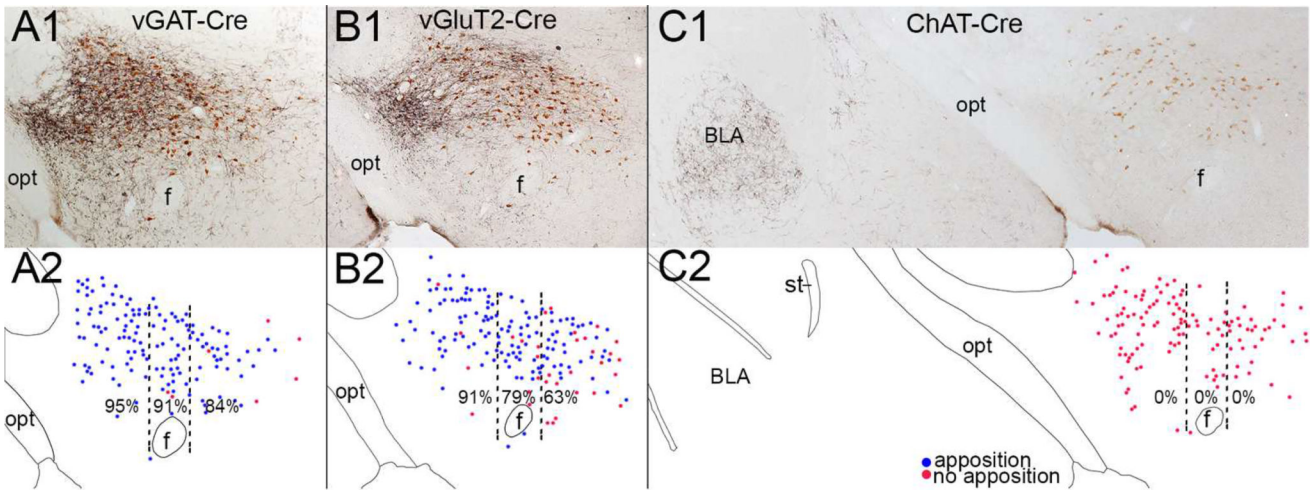

Figure 5. Variations in SI appositions across the orexin field

(A–B) In vGAT-cre and vGluT2-cre mice, mCherry-labeled SI fibers (black) heavily innervate the orexin neurons (brown). **(C)** In Chat-cre mice, cholinergic fibers from the SI do not innervate the orexin neurons, but they heavily innervate the basolateral amygdala (BLA). **(A2–C2)** Drawings of the above photos showing the pattern of orexin neurons apposed (blue dots) or not apposed (red dots) by SI terminals from individual mice. Percentages are the mean number of orexin neurons with appositions in the lateral, perifornical, and medial parts of the orexin field across three mice of each cre line.

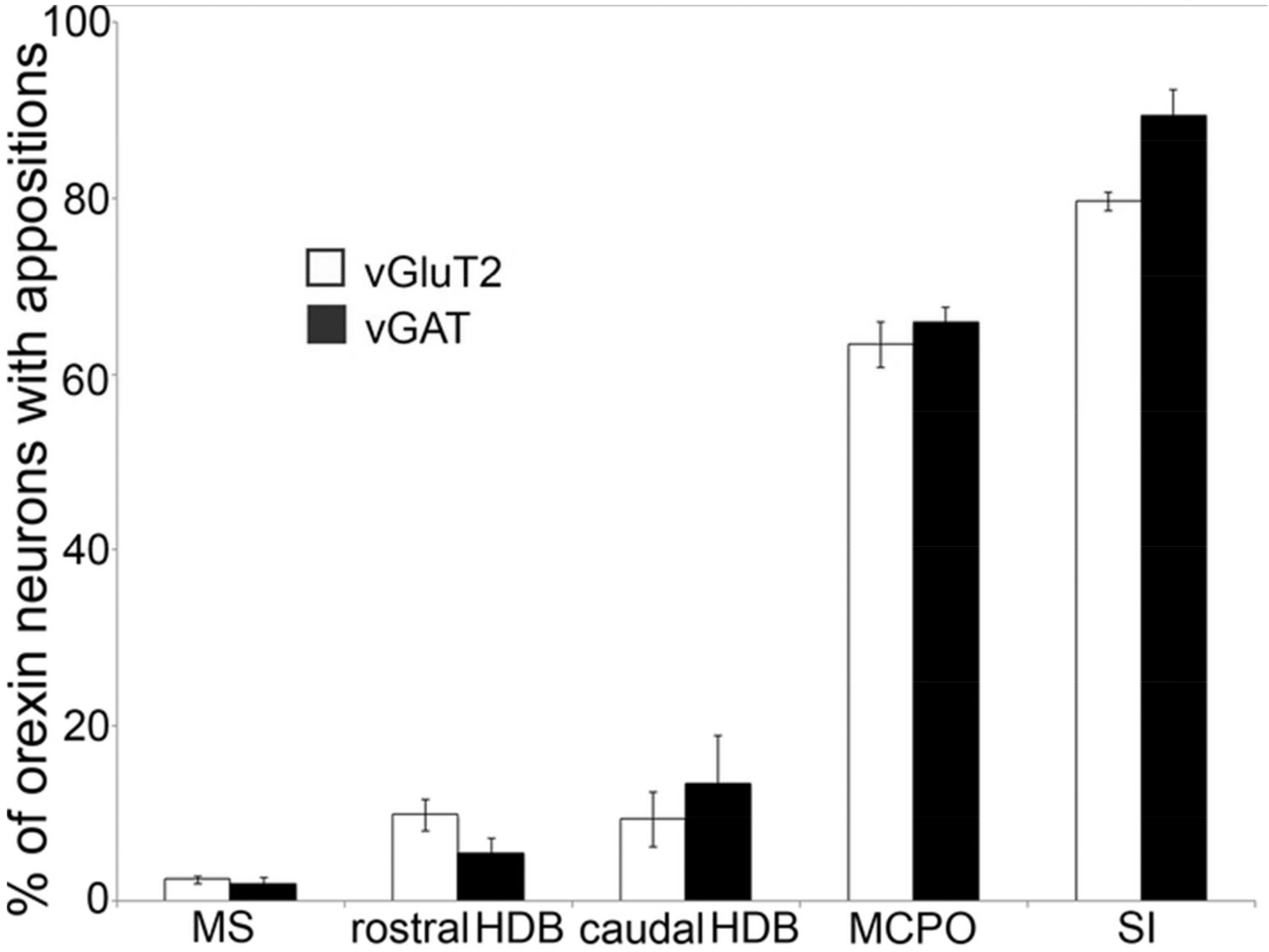

Figure 6. Percentage of orexin neurons with appositions from different BF regions and cell types

SI and MCPO heavily innervate the orexin neurons while MS and HDB innervation is minimal.

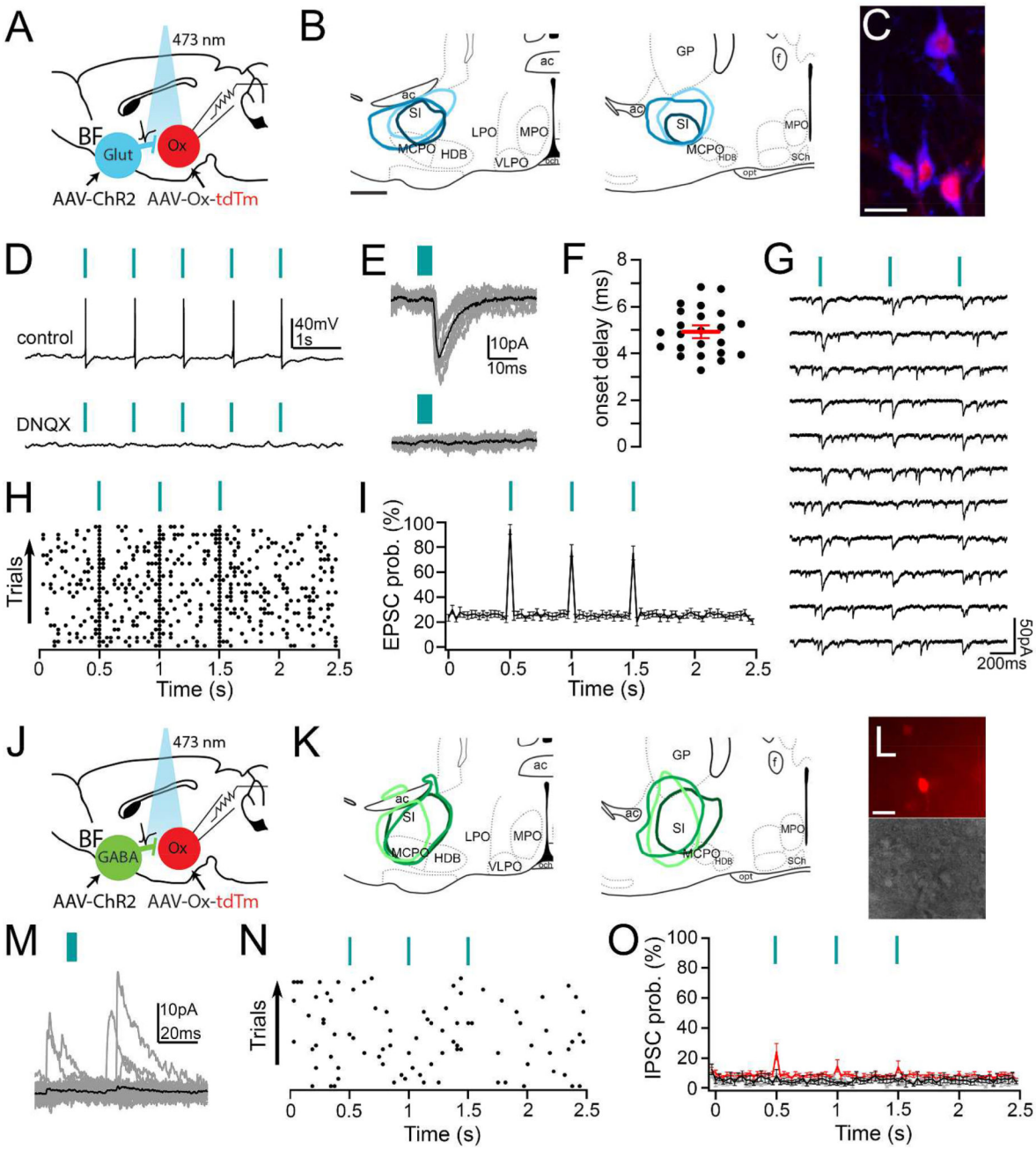

Figure 7. Channelrodopsin-2-assisted circuit mapping (CRACM) to test functional connectivity of SI projections to the orexin neurons

(A) We injected AAV-ChR2-YFP (AAV-ChR2) into the SI of vGluT2-Cre mice, and we injected AAV-horexin-tdTomato (AAV-Ox-tdTm) in the ipsilateral orexin field to label orexin neurons. We recorded from orexin neurons that expressed tdTomato and used blue light pulses to stimulate glutamate release from SI glutamatergic terminals. (**B)** Three representative AAV-ChR2-YFP injection sites used for CRACM (scale bar = 500 μm). **(C)** After injection of AAV-horexin-tdTomato, lateral hypothalamic neurons are labeled for orexin-A (pseudocolored blue) and tdTomato (red), scale bar = 20 μm. **(D)** Photostimulation

of glutamatergic inputs from the SI reliably evokes action potentials in orexin neurons that are blocked by DNQX 20 μM (current clamp recordings; blue lines signify 5 ms light pulses). **(E)** Photostimulation also evokes glutamatergic EPSCs in orexin neurons that are blocked by DNQX (bottom trace) (voltage-clamp recordings Vh = −60 mV; grey traces are single trials; black are the average responses). **(F)** Photostimulation evokes very short latency EPSCs (black dots are mean latencies in individual orexin neurons; red line is the population mean ± SEM; n = 23). **(G)** Photo-evoked EPSCs recorded in TTX (1 μM + 4-AP 1 mM), indicating monosynaptic connectivity. **(H)** Raster plot of glutamatergic EPSCs in orexin neurons after three light pulses (30 ms bins). **(I)** Average EPSC probability was high in 23 out of 25 recorded orexin neurons with three light pulses. **(J)** We injected AAV-ChR2-YFP into the SI of vGAT-Cre mice, and used 5 ms blue light pulses to stimulate GABA release from SI GABAergic terminals. **(K)** Schematic of three representative AAV-CHR2-YFP injections used for CRACM in vGAT-cre mice. **(L)** An example of a recorded slice containing orexin neurons expressing tdTomato (top) and visualized under IR-DIC system during whole-cell recordings (scale bar: 25 μm). **(M)** Orexin neurons receive spontaneous GABAergic IPSCs, but these events are not synchronized to the photostimulation of the GABAergic terminals (voltage clamp traces in a representative orexin neuron recorded with the K-gluconate based pipette solution, Vh = 0 mV). **(N)** Raster plot of GABAergic IPSCs in an orexin neuron after three light pulses. **(O)** Three light pulses did not increase the average IPSC probability in all 5 orexin neurons recorded with the K-gluconate based pipette solution (grey trace) or in all 8 orexin neurons recorded in Cs-methane-sulfonate-based pipette solution (black trace). Light pulses induced IPSCs in only 4 out of 26 orexin neurons recorded with the KCl-based pipette solution (red trace).

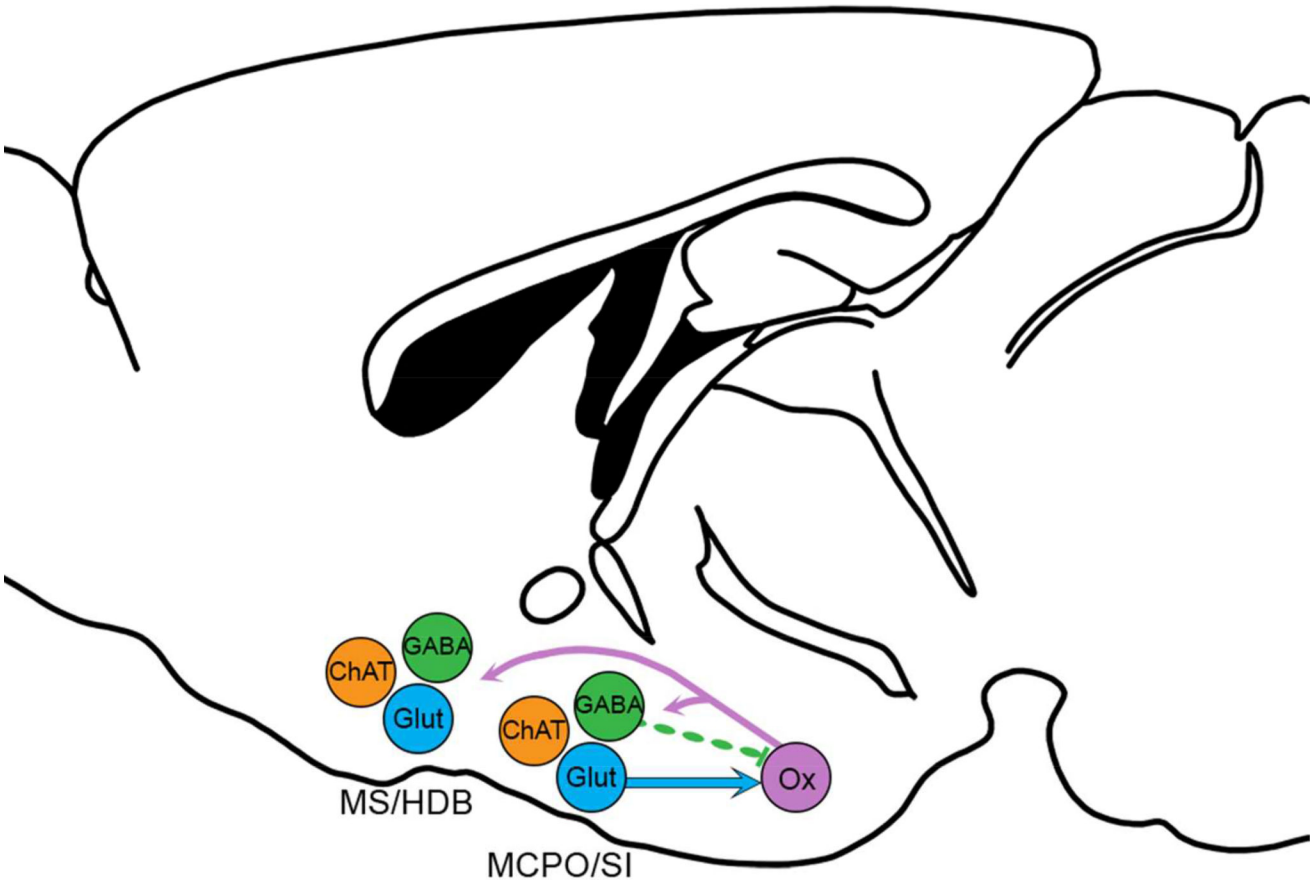

Figure 8. Schematic of BF projections

Reciprocal projections between the BF and orexin neurons. Previous studies show that the orexin neurons innervate cholinergic and non-cholinergic neurons of the entire BF. Glutamatergic (Glut) neurons of the MCPO and SI heavily innervate and excite the orexin neurons. GABAergic (GABA) neurons of these regions project heavily to the orexin neurons but rarely form functional synapses on orexin neurons. Non-cholinergic projections from the MS and HDB are light. Cholinergic (ChAT) BF neurons do not project to the orexin neurons.

TABLE 1

Details on antisera used in these experiments.

Antigen	Immunogen	Manufacturer, catalog or lot number, the RRID species, mono or poly	Concentration
Orexin A	a peptide mapping at the C-terminus of human orexin-A	Santa Cruz Biotechnology, Cat# sc-8070, RRID:AB_653610, goat, polyclonal	1:10,000 for DAB, 1:5,000 for fluorescence
ChAT	Human placental enzyme	Millipore, Cat# AB144P-1ML, RRID:AB_262156, goat, polyclonal	1:2,000 for DAB, 1:1,000 for fluorescence
DsRed	DsRed-Express, a variant of Discosoma sp. red fluorescent protein.	Clontech, Cat# 632496, RRID:AB_10013483, rabbit, polyclonal	1:5,000 for DAB, 1:2,000 for fluorescence
GFP	GFP from Aequorea victoria.	Life Technologies, A10262, RRID:AB_11180610, polyclonal	1:5,000

Table 2

Glutamatergic and GABAergic axon terminals from the MCPO and SI appose a large number of orexin neurons, but axons from more rostral and medial parts of the basal forebrain do not. Values are the total number of orexin neurons across three sections, averaged across three animals.

vGluT2		
	Orexin neurons	**Orexin neurons with appositions**
MS	207 ± 5	5 ± 1
Rostral HDB	203 ± 9	19 ± 3
Caudal HDB	284 ± 24	30 ± 3
MCPO	245 ± 13	155 ± 5
SI	283 ± 8	226 ± 7

vGAT		
	Orexin neurons	**Orexin neurons with appositions**
MS	271 ± 40	6 ± 3
Rostral HDB	226 ± 9	12 ± 2
Caudal HDB	277 ± 12	47 ± 5
MCPO	255± 41	170 ± 17
SI	245 ± 18	220 ± 20

	SI GluT2	SI vGAT	HDB vGluT2	HDB vGAT	MS vGluT2	MS vGAT
Thalamus						
MD	++	++	-	-	-	-
PVT	+	-	-	-	-	-
LHb	+++	+	+	+	-	-
mHb	-	-	-	+++	-	++
Amygdala						
BLA	-	+	-	-	-	-
CEL	-	-	-	-	-	-
CEM	++	++	-	-	-	-
BMA	+	++	-	-	-	-
Hypothalamus						
LH	++	++	+	+	-	-
SUM	+++	+++	-	+++	++	-
MM	-	-	-	+++	-	-
STh	-	-	-	-	-	-
PSTh	+++	+++	-	-	-	-
Midbrain						
VTA	+++	+++	-	-	-	-
SNR	-	-	-	-	-	-
SNC	++	++	-	-	-	-
DpME	+++	+++	-	-	-	-
interpeduncular	-	-	-	+++	-	-
Brainstem						
VLPAG	+	+	-	-	-	-
PPT	+/-	+/-	-	-	-	-
PB	++M	+++ML	-	-	-	-
LDT	+	+	-	+	-	-
dorsal raphe	++	++	+	+	+	+
median raphe	+	+	-	+++	+	+
LC	+	+	-	-	-	-
pontine cent. grey	+	+	-	++	+	+
IRt	+	+	-	-	-	-
parvicellular retic. nucleus	-	+	-	-	-	-
medullary retic.	-	+	-	-	-	-